



Research Article

Open Access

Sonia Alejandra Torres-Sánchez*, Carita Augustsson, Uwe Jenchen, J. Rafael Barboza-Gudiño, Eduardo Alemán Gallardo, Juan Alonso Ramírez Fernández, Darío Torres-Sánchez, and Michael Abratis

Petrology and geochemistry of meta-ultramafic rocks in the Paleozoic Granjeno Schist, northeastern Mexico: Remnants of Pangaea ocean floor

<https://doi.org/10.1515/geo-2017-0029>

Received September 19, 2015; accepted July 5, 2017

Abstract: The Granjeno Schist is a meta-volcano-sedimentary upper Paleozoic complex in northeastern Mexico. We suggest different tectonic settings for metamorphism of its serpentinite and talc-bearing rocks based on petrographic and geochemical compositions. According to the REE ratios ($\text{La}_N/\text{Yb}_N = 0.51\text{--}20.0$ and $\text{La}_N/\text{Sm}_N = 0.72\text{--}9.1$) and the enrichment in the highly incompatible elements Cs (0.1 ppm), U (2.8 ppm), and Zr (60 ppm) as well as depletion in Ba (1 – 15 ppm), Sr (1 – 184 ppm), Pb (0.1 – 14 ppm), and Ce (0.1 – 1.9 ppm) the rocks have mid-ocean ridge and subduction zones characteristics. The serpentinite contains Al-chromite, ferrian chromite and magnetite. The Al-chromite is characterized by Cr# of 0.48 to 0.55 suggesting a MORB origin, and Cr# of 0.93 to 1.00 for the ferrian chromite indicates a prograde metamorphism. We propose at least two serpentinization stages of lithospheric mantle for the ultramafic rock of the Granjeno Schist, (1) a first in an ocean-floor environment at sub-greenschist to greenschist facies conditions and (2) later a serpentinization phase related to the progressive replacement of spinel by ferrian chromite and magnetite at greenschist to low amphibolite facies conditions during regional metamorphism. The second serpentinization phase took place in an active continental margin during the Pennsylvanian. We propose that the origin of the ultramafic rocks is related to an obduction and accretional event at the western margin of Pangea.

Keywords: ultramafic rocks; serpentinite; Granjeno Schist; northeastern Mexico, Gondwana, Pangea

1 Introduction

In Mexico, details of the Laurentia-Gondwana collision remain controversial [1]. Even though several studies have examined the Paleozoic (Silurian to Carboniferous) basement rocks of northeastern Mexico, [2–11] the evolution of the ultramafic paleozoic rocks has received minor attention; therefore this topic should be furtherly studied [11–18]. It is commonly accepted that metamorphism including serpentinization of the Granjeno Schist, a metavolcanic and metasedimentary unit of 300 ± 4 Ma metamorphic age, was related to the closure of the Rheic Ocean and the resulting formation of Pangaea.

The protoliths of the Granjeno Schist indicate different tectonic setting of formation. Most recently, Torres [19] suggest that N-MORB rocks indicates extrusion along a mid-ocean ridge related to the rifting and drifting of the Rheic Ocean during Silurian to Devonian time, whereas

C.P. 78290, San Luis Potosí, S. L. P., México, E-mail: soniatorres-san@hotmail.com

Carita Augustsson: Institutt for Petroleumsteknologi, Universitetet i Stavanger, 4036 Stavanger, Norway

Uwe Jenchen, Eduardo Alemán Gallardo, Juan Alonso Ramírez Fernández: Universidad Autónoma de Nuevo León, Avenida Universidad S/N, Ciudad Universitaria, C.P. 6645, San Nicolás de los Garza, Nuevo León, México

and Facultad de Ciencias de la Tierra, UANL, Hacienda de Guadalupe, Carretera a Cerro Prieto, km 8, C. P. 67700 Linares, Nuevo León, México

J. Rafael Barboza-Gudiño: Instituto de Geología Universidad Autónoma de San Luis Potosí, Manuel Nava No. 5. Zona Universitaria, 78240 San Luis Potosí, S. L. P., México

Michael Abratis: Brücker Nano, Am Studio 2D, 12489 Berlin, Alemania

Darío Torres-Sánchez: Instituto Potosino de Investigación Científica y Tecnológica A.C., Camino a La Presa de San José 2055, Lomas 4 sección, 78216 San Luis, S.L.P.

*Corresponding Author: Sonia Alejandra Torres-Sánchez:

Facultad de Ingeniería, Universidad Autónoma de San Luis Potosí, Dr. Manuel Nava No. 8, Col. Zona Universitaria Poniente,

enriched basaltic rocks indicate mixing of MORB magma with an enriched deep mantle source. The magmatism was probably associated with plate movements related to the closure of the Rheic Ocean, supporting the migration of the southwestern margin of Gondwana into the Paleo-Pacific Ocean [20, 21]. The southwestern margin of Gondwana changed from passive to active with the development of an oblique subduction system during the Pennsylvanian [14, 18, 22]. Based on field relationships, petrographic and isotopic characterization of metasedimentary and metavolcanic rocks, it is possible to estimate that the Granjeno Schist was integrated and metamorphosed in an accretionary prism during this time [1, 13, 14, 17, 18, 23–25]. No particular attention has been entirely paid to the significance of the serpentinite bodies within the Granjeno Schist. Hence, until now the relation between the protoliths of the metasedimentary, metavolcanic and meta-ultramafic rocks and their plate-tectonic setting has not been considered for the evolution of northwestern Gondwana.

Since the 1970's serpentinite and talc bodies within the Granjeno Schist have been reported in the area of northeastern Mexico [26, 27]. Their origin has been interpreted 1) as a result of diapiric upwelling, 2) part of an ophiolite, 3) a sheeted dike layer and/or 4) having a subduction relation. These interpretations were mostly founded on field and petrographic observations in the Novillo Canyon and less from the Peregrina Canyon, both in northeastern Mexico [5, 8, 10, 14, 28–30]. Talc-bearing rocks and serpentinite also occur in the Aramberri Uplift but no studies exist on their origin.

The present study constitutes the first detailed work dealing with the petrology and geochemistry of Paleozoic serpentinite and associated talc-bearing rocks in northeastern Mexico. The purposes of the study are to: a) establish the tectonic setting of the serpentinite protoliths, b) determine the metamorphic conditions that affected the rocks, as well as c) establish a geological model for the evolution of late Paleozoic tectonic events in northeastern Mexico during Pangaea configuration. In order to achieve this, we use criteria based on primary and secondary mineralogical compositions, and mineral and whole-rock chemistry of the serpentinite of the Granjeno Schist.

2 Geological Setting

During Late Carboniferous and early Permian times Gondwana and Laurentia collided to form the supercontinent Pangaea [31, 32] separating several small terranes from

Gondwana and accreted to Laurentia [33–35]. Remnants of the late Paleozoic Rheic Ocean closure and consequent collision between Laurentia and Gondwana are scarce, but not absent in Mexico. Visible vestiges of the Rheic Ocean include the Paleozoic rocks of the Granjeno Schist in northeastern Mexico. The origin of these rocks is closely linked to the outboard margins of the microcontinent Oaxaquia during the configuration of Pangaea (Fig. 1a; [14]). These rocks demonstrate that the closure of the Rheic Ocean, in the area of actual northeastern Mexico, did not result in continent-continent collision during the middle to late Paleozoic. It rather brought the northwestern margin of Gondwana into contact with the Paleo-Pacific Ocean [18, 19, 36, 37].

The Granjeno Schist is a poly-deformed metavolcano-metasedimentary sequence that includes both sedimentary (psammite, pelite, turbidite, conglomerate, black shale) and igneous (tuff, lava flows, pillow lava, ultramafic bodies) protoliths that have been metamorphosed under sub-greenschist to greenschist facies conditions [2–4, 8, 11, 13, 19].

2.1 Regional distribution of the Granjeno Schist

The Granjeno Shist crops out in axes of anticlines in the Sierra Madre Oriental in northeastern Mexico, e.g., in the Huizachal-Peregrina anticlinorium. This N-NW-trending, double plunging structure is located northwest of Ciudad Victoria in Tamaulipas (Fig. 1b; [38]), where the Granjeno Schist forms two major NW-trending blocks.

In the southwestern block a major NW-SE trending dextral fault separates the Granjeno Schist from the Mesoproterozoic Novillo Gneiss. A body of plagiogranite [8] with an intrusion age of 351 ± 54 Ma (U-Pb in zircon) and a cooling age of 313 ± 7 Ma ($^{40}\text{Ar}/^{39}\text{Ar}$ in muscovite, [13]), is located in the fault contact. The Granjeno Schist northeastern block is in fault contact with Permian flysch and redbeds. In the south-central portion of the Huizachal-Peregrina anticlinorium, an elongate serpentinite body within the Granjeno Schist is in tectonic contact with metasedimentary and metavolcanic rocks.

Other, isolated outcrops of the Granjeno Schist are present in the Miquihuana and Bustamante Uplift (Tamaulipas) areas southwest of the Huizachal-Peregrina anticlinorium (Fig. 1b), and in the Aramberri Uplift, Nuevo Leon (Fig. 1b), in tectonic contact with small lenses of serpentinite and talc bodies. In all parts these units are overlain by Early Jurassic volcanic rocks, Early-Late

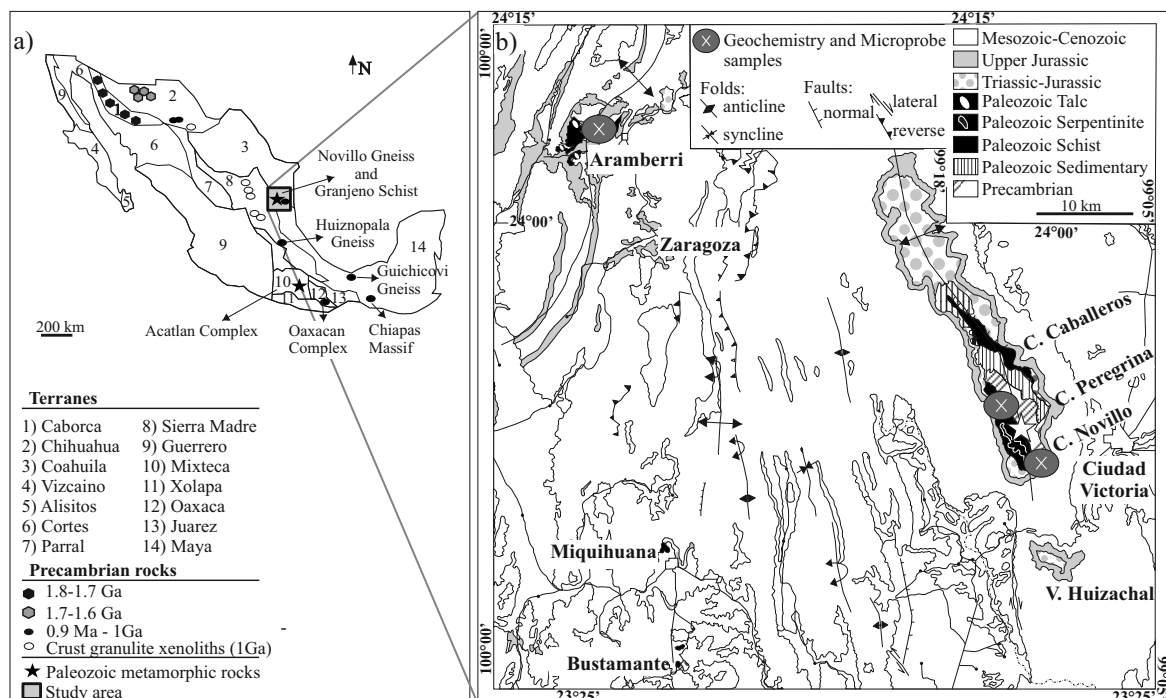


Figure 1: a) Precambrian and Paleozoic metamorphic rocks in Mexico. Modified from Ortega et al. [9] b) Study area (after [18]) with the the Granjeno Schist.

Jurassic rift, drift and passive margin sediments related to the opening of the Gulf of Mexico basin [39–43].

The metamorphic age of the Granjeno Schist rocks of the Huizachal-Peregrina anticlinorium has been investigated in several studies. Most recently, [19] reported a $^{40}\text{Ar}/^{39}\text{Ar}$ plateau age on phengite of 300 ± 4 Ma in the metavolcanic rocks from the Peregrina Canyon. This age is equivalent with the reported age of $^{40}\text{Ar}/^{39}\text{Ar}$ in phengite of the metasedimentary rocks from the Novillo Canyon [13]. Older Rb-Sr whole-rock muscovite isochron ages in metasediments range from 318 ± 10 Ma to 257 ± 8 Ma [3, 44]. Whole-rock Rb-Sr ages of 373 ± 37 Ma to 320 ± 12 Ma are recalculated from [27, 45, 46]. The metasedimentary rocks from the Aramberri Uplift yield muscovite K-Ar ages from 270 ± 5 to 294 ± 6 Ma [26].

2.2 Description of the meta-ultramafic rocks

The serpentinite bodies in the Huizachal-Peregrina anticlinorium are up to 500 m thick and 10 km long (Fig. 1b). In the Novillo and Peregrina Canyons the serpentinite rocks occur in layers of 10 cm to 500 m in thickness (Fig. 2a). The serpentinite consists of foliated to massive, greenish and lustrous rocks. In places it is possible to recognize

dark and clear green-banded texture and pillow structures as protolith remnants. The metacumulate in the Novillo Canyon is a coarse-grained, dark green rock. It is intensively fractured in lateral fault contact with the serpentinite bodies. At both localities the serpentinite rocks are in sub-vertical fault contact with other metasedimentary and metavolcanic rocks of the Granjeno Schist. The foliation of the serpentinite is parallel to the schistosity of the surrounding low-grade metamorphic rocks.

In the Aramberri uplift, serpentinite lenses are 10 cm thick and 1 m long and are associated with talc bodies up to 50 cm thick and 30 m long. The talc bodies can be distinguished from the other lithologies due to its grayish to pearly color and softness. The talc bodies occur in fault contact with the metasedimentary rocks (Fig. 2b). In this area serpentinite is present in shear zones.

3 Sampling and analytical methods

Twenty one samples of serpentinite, metacumulate and talc-bearing rocks from the Novillo and Peregrina Canyons, as well as one soapstone sample from the Aramberri Uplift, were analyzed (Table 1). Petrographic

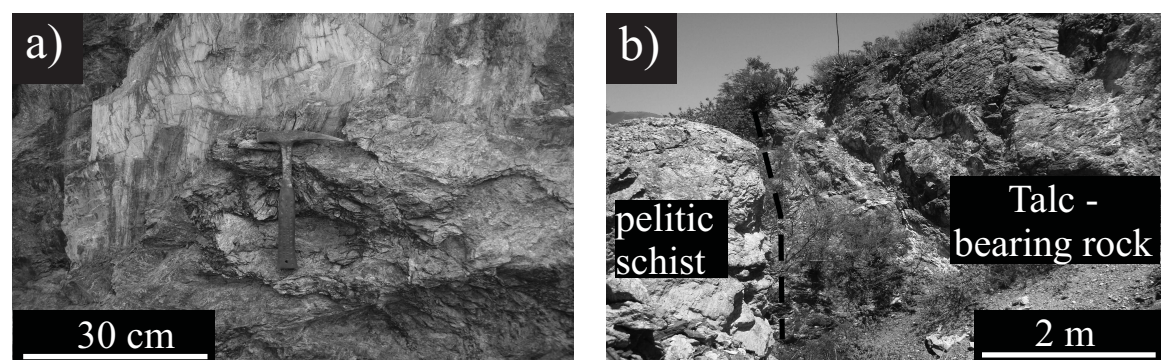


Figure 2: a) Serpentinite from the Novillo Canyon with acicular texture, b) lateral contact of talc body with pelitic schist in the Aramberri Uplift.

Table 1: Coordinates, lithology, mineral content and methods of the studied metaultramafic samples from Granjeno Schist.

Sample	Location	Coordinates (WGS 84)	Lithology	Mineralogy	Method
MS1	NC	140471798E, 262486N	Serpentinite	Lz+Mg+Chr+Stch	GC
MS2	NC	140471741E, 2622455N	Serpentinite	Lz+Mg+Chr+Stch+Chl+Chr	GC
MS3	NC	140471742E, 2622460N	Serpentinite	Lz+Mg+Chr	GC
MS4	NC	140471880E, 2623442N	Serpentinite	Lz+Czo+Ctl+Mg+Chr	GC
MS5	NC	140471713E, 2622424N	Serpentinite	Lz+Mg+Chr+Stch+Chl+Chr	GC
MS6	NC	140471713E, 2622426N	Serpentinite	Lz+Mg+Chr	MP
MS7	PC	140468618E, 2627290N	Serpentinite	Lz+Mg+Chr+Stch+Chl+Chr	GC
MS8	PC	140468616E, 2627285N	Serpentinite	Lz+Mg+Chr+Stch+Chl+Chr	GC
MS9	PC	14046893E, 2627654N	Serpentinite	Lz+Ctl+Do	GC
MS10	PC	140468616E, 2627280N	Serpentinite	Lz+Ca+Pn+Mg+Chr	GC, MP
MS11	PC	140468616E, 2627285N	Serpentinite	Lz+Ca+Pn+Mg+Chr	GC
MC1	NC	140472424E, 2623276N	Metacumulate	Chl+Ab+Cpx+Grs+Qz	GC, MP
MT1	NC	140472194E, 2622918N	Talc	Lz+Mg+Chr+Ta	GC
MT2	NC	140471763E, 2623374N	Talc/serpentine	Ca+Tr+Chl+Srp	GC, MP
MT3	PC	140468973E, 2627246N	Talc-serpentine	Ta+Atg	GC
MT4	AU	140415564E, 2668563N	Talc	Qz+Ta+Ca+Chl	GC
MT5	AU	140408800E, 2666595N	Talc-serpentine	Ta+Chl+Ca+Qz+Pn	MP
MT6	AU	140415346E, 2667980N	Talc	Ta+Srp	MP

Ab: albite, Atg: antigorite, Ca: calcite, Chl: chlorite, Chr: chromite, Cpx: clinopyroxene, Ctl: Chrysotile, Do: dolomite, Grs: grossular, Lz: lizardite, Mg: magnetite, Qz: quartz, Ta: talc, Czo: clinozoisite, Pn: pentlandite, Stch: stichite, AU: Aramberri Uplift, NC: Novillo Canyon and PC: Peregrina Canyon, MP: Microprobe analysis, GC: geochemical analysis.

analyses were accomplished for all samples with a polarizing microscope.

Chemical compositions of minerals were analyzed with the electron microprobe JEOL JXA 8230 at the Institute of Geosciences of the Friedrich-Schiller University, Jena, Germany. Serpentine, chlorite, talc, amphibole, pyroxene, chromite, pentlandite, magnetite and garnet compositions (Appendices 1–9) were determined from samples

of all three study areas. The microprobe acceleration voltage was 15.0 kV and the beam current was 15 nA. A beam size of 2–3 µm was used. All standards were certified silicates and oxides.

Total abundances of major oxides and trace elements were measured for fifteen samples: ten serpentinite, one metacumulate, three talc-bearing rock and one soapstone sample (Table 1). They were powdered in an agate mill and

analyzed with ICP-OES (major element oxides) and ICP-MS/INAA (Cr, Ni, Co, V, Cu, Pb, Zn, Rb, Ba, Sr, Ga, Nb, Hf, Cs, Ta, Th, U, Zr, Y and REE) with an accuracy of $+/- 5$ to 20 % at Acmelab (Vancouver, Canada).

Metamorphic temperatures for the meta-ultramafic rocks were determined using the chlorite thermometer of [47], which is based on Al^{IV} in chlorite and compared with the corrected thermometer by [48]. The temperature calculation considers the influence of iron in chlorite, and requires that $\text{Fe}/(\text{Fe}+\text{Mg}) < 0.6$. The Appendices 1–10 provide mineral and whole-rock chemical compositions and a list of compositional preconditions for the calculated metamorphic conditions.

4 Results

4.1 Petrographic outlines

The meta-ultramafic rocks are mainly composed of the metamorphic minerals serpentine, chlorite, talc, amphibole and garnet. The opaque phases chromite, magnetite and pentlandite are also present. Relic clinopyroxene is recognizable.

The serpentinite rocks in all areas have four different textures: a) acicular texture consisting of fibrous lizardite and chlorite with crystal sizes up to 0.25 mm, b) pseudomorphic bastitic texture including bastite in crystals up to 1 mm in size, mainly as an alteration product from clinopyroxene, and with chrysotile and chlorite rims about 0.3 mm wide (Fig. 3a), c) box work texture consisting of acicular cross antigorite (Fig. 3b), and d) mesh texture conformed by ribbons of lizardite and antigorite and replaced in its core by carbonate and/or talc. In general the opaque phases in the serpentinite are granular and fractured, up to 0.4 mm and with chrysotile and stichtite veins. Veins and ribbons of antigorite are recognizable in all serpentinite. Also talc occurs as vein filling in the serpentinite from the Novillo and Peregrina Canyons.

In the serpentinite the recognizable opaque phases as spinel crystals occur in irregular protogranular to amoeboidal shapes. They are present in the serpentinite from the Peregrina and Novillo canyons. The spinel is present as a) crystals of homogeneous deep red color, b) zoned, deep red crystals with a black outer rim and c) homogeneous black crystals. The homogeneous deep red spinel crystal and some cores of the zoned crystals have preserved the primary spinel composition. Magnetite occurs as rim/rim boundaries in chromite and ferrian chromite (Fig. 3c) and as irregular crystals (Fig. 3d) in mesh textures and within

mesh cores. Pentlandite occurs in protogranular and fractured shapes (Fig. 3e).

In the metacumulate, relic porphyroclasts of bent and kinked diopside up to 6 mm in size are surrounded by subhedral crystals of recrystallized diopside, tabular amphibole, polygonal grossular (Fig. 3f) and tabular and elongated chlorite.

The talc-bearing rocks have fibrous and nematoblastic texture. They are dominated by tabular porphyroblasts of pure talc of 0.3 mm to 0.5 mm in size which are associated with orthopyroxene and replaced serpentine, uncolored, greenish and brownish subhedral tremolite (Fig. 3g), associated with chlorite and secondary dolomite and granular calcite (≤ 0.33 mm to 0.5 mm; Fig. 3h). The groundmass consists of fibrous talc and chlorite (≤ 0.15 mm; Fig. 3g, h, i).

4.1.1 Mineral content and its chemical composition

4.1.1.1 Serpentine

The serpentine from the Novillo and Peregrina Canyons have SiO_2 contents that vary from 37 to 45 wt%, MgO from 35 to 41 wt%, FeO from 1.6 to 7.2 wt%, Al_2O_3 from 0.56 to 4.8 wt% and Cr_2O_3 of 1.2 to 5.9 wt%. The serpentine from the Aramberri Uplift has lower SiO_2 with 29 to 32 wt% and MgO of 25 to 26 wt%, higher FeO of 11.0 to 11.9 wt%, Al_2O_3 of 14 to 17 wt% and Cr_2O_3 of 1.2 to 2.1 wt% (Appendix 1). The $\text{Mg}/(\text{Mg}+\text{Fe}^{2+})$ ratio varies from 0.90 to 0.98 for the Novillo and Peregrina canyons-rocks and from 0.80 to 0.91 for the Aramberri Uplift rocks. All analyzed serpentine has Mg/Si values between 1.2 and 1.5.

4.1.1.2 Chlorite

$\text{Fe}/(\text{Fe}+\text{Mg})$ is *c.* 0.1 and Si is 3.0 apfu for the chlorite in the metacumulate. Chlorite in the talc-bearing rocks and the soapstone of the Novillo Canyon has $\text{Fe}/(\text{Fe}+\text{Mg})$ of 0.2 and Si of 4.2 apfu. These values classify the chlorite as clinochlore and talc-chlorite. Higher $\text{Fe}/(\text{Fe}+\text{Mg})$ ratios of *c.* 0.25 to 0.30 and Si of 2.9 to 3.5 apfu for talc at Aramberri Uplift classify the mineral as pycnochlorite (Appendix 2).

4.1.1.3 Chlorite geothermometer

The tetrahedral Al (AlIV) content in chlorite is 0.93 to 1.05 apfu for the metacumulate of the Novillo Canyon. This corresponds to crystallization temperatures of 253–276°C with a mean of 268°C (*n* = 4; Appendix 2; cf. [47]). The $\text{Fe}/(\text{Fe}+\text{Mg})$ ratios of < 0.6 are taken into account for temperature calculations according to [48] Jowett (1991). This

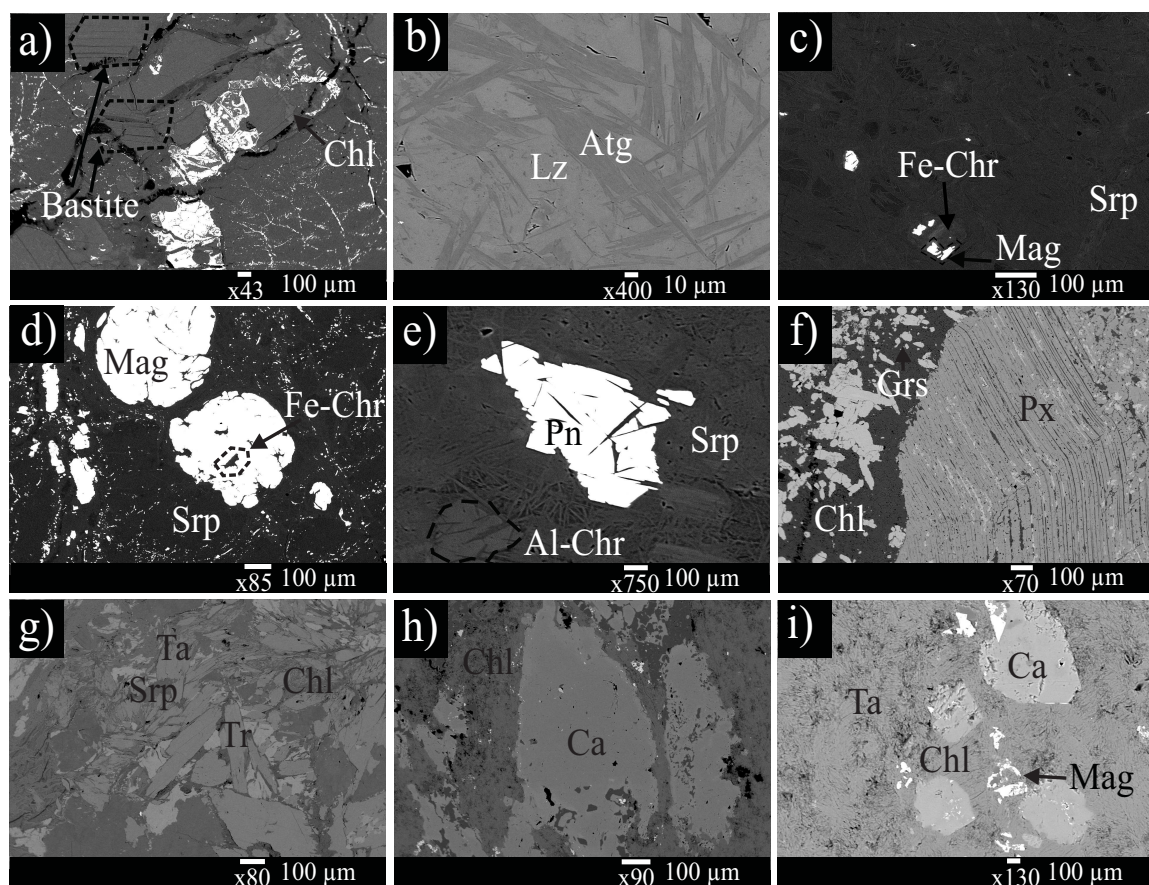


Figure 3: Scanning-electron-microscope images a) Pseudomorphic bastitic texture, b) box work texture with acicular antigorite and lizardite matrix, c) chromite and ferrian chromite with magnetite rims in serpentinite, d) rounded magnetite with chromite cores in serpentinite, e) protoprotomylonitic and fractured pentlandite in serpentinite, f) metacumulate with relic porphyroclasts of bent and kinked diopside and polygonal grossular, g) nematoblastic texture dominated by porphyroblasts of talc, tremolite in fibrous talc and chlorite matrix h) talc and chlorite groundmass and i) granular calcite and magnetite in talc-bearing rock. Al-Chr: aluminium chromite, Atg: antigorite, Ca: calcite, Chl: chlorite, Fe-Chr: iron rich chromite, Grs: grossular, Lz: lizardite, Mag: magnetite, Pn: pentlandite, Px: pyroxene, Srp: serpentine, Ta: talc, Tr: tremolite.

gives temperatures that are 1–30°C higher than the temperatures derived from the [47] thermometer (Appendix 2).

$Mg/(Mg+Fe^{2+})$ ratio is very high with values of 0.90–0.92 (Appendix 5).

4.1.1.4 Pyroxene

The clinopyroxene has a limited compositional range of diopside with Wo_{45–50}En_{43–50}Fs_{5–15} (Appendix 3).

4.1.1.5 Garnet

It has a grossular composition of Py_{8–14}Alm_{3–6}Gs_{80–88} (Appendix 4) and is associated with diopside and chlorite.

4.1.1.6 Talc

The talc has Si content of 7.7 apfu, Mg of 4.02 to 4.09 apfu, low Fe of 0.37 to 0.43 apfu and Al of < 0.07 apfu. The

4.1.1.7 Amphibole

The chemical composition is calcic, dominated by tremolite $Mg/(Mg+Fe^{2+}) = 0.93–0.98$, actinolite $Mg/(Mg+Fe^{2+}) > 1$ and ferroactinolite $Mg/(Mg+Fe^{2+}) \leq 1$; Appendix 6). The coexistence of these amphibole minerals suggests progressive metamorphism (cf. [49]).

4.1.1.8 Spinel

They have low Cr# ($Cr/(Cr+Al)$) values of 0.48 to 0.55, high $Mg/(Mg+Fe^{2+})$ ratios of 0.57 to 0.71 and low TiO_2 of < 0.37 wt%. Spinel composition data of [10], from the Novillo Canyon reveal Cr^{3+} of 0.64 to 0.65 apfu, Fe^{3+} of 0.33–0.53

apfu and Al^{3+} of 0.01 apfu, which classify this mineral as Al-chromite (*cf.* [50]).

Among the measured spinel, outer rims and homogeneous black crystals have Cr# values of 0.93 to 1.00, $\text{Mg}/(\text{Mg}+\text{Fe}^{2+})$ ratios varies from 0.01 to 0.52 and TiO_2 from 0.16 to 0.59 wt%, similar to metamorphic spinel in supra-subduction zones (*cf.* [51]). Their Cr^{3+} values of ≤ 0.53 apfu, Fe^{3+} values of 0.46–0.93 apfu and Al^{3+} values of ≤ 0.04 apfu correspond to the alteration of the chromite (Fig. 4 (*cf.* [52], Appendix 7).

4.1.1.9 Magnetite

According to Cr^{3+} values of ≤ 0.66 apfu, Fe^{3+} values of 1.33–1.98 apfu and depletion in Al^{3+} , the magnetite can be classified as pure magnetite (Fig. 4) and Cr-rich magnetite. Cr# values range from 0.99 to 1.00, $\text{Mg}/(\text{Mg}+\text{Fe}^{2+})$ varies from 0.02 to 0.25 and TiO_2 from 0.01 to 0.20 wt% (Appendix 8).

4.1.1.10 Pentlandite

It is associated with lizardite and antigorite. It has FeO of 31.8 to 37.1 wt% (Appendix 9).

4.2 Whole-rock geochemical composition

4.2.1 Major-element composition

All studied serpentinite rocks have high loss on ignition values of > 10 wt%, indicating high water contents. The samples corresponds to almost pure serpentinite rocks. The metacumulate and talc-bearing rocks have loss on ignition values of < 5 wt% (Appendix 10).

The serpentinite rocks from the Peregrina Canyon has MgO of 34–35 wt%, SiO_2 of 38–43 wt%, FeO of 6.7–7.5 wt%, Al_2O_3 of 1.0–1.5 wt% and CaO of < 2.3 wt%. The serpentinite from the Novillo Canyon has lower MgO with 16–39 wt%, SiO_2 of 36–45 wt%, FeO of 2.6–11 wt%, Al_2O_3 of 0.8–13 wt% and higher CaO of < 22 wt%. The Mg# ($(\text{MgO}_{\text{mol}})/(\text{MgO}_{\text{mol}} + \text{FeO}_{\text{tot}}) \times 100$) is similar for both areas with 85–98.

The metacumulate from the Novillo Canyon has MgO of 15 wt%, SiO_2 of 40 wt%, FeO of 2.4–11 wt%, Al_2O_3 of 14 wt% and CaO of < 22 wt%. The high concentration of CaO in the metacumulate is in accordance with the presence of clinopyroxene and garnet. The high Al_2O_3 is related to the presence of chlorite. Its Mg# of 69 is lower than in the serpentinite.

In accordance with Al_2O_3 of < 0.13 , CaO of < 0.45 and MgO of 0.30–0.97 in mole%, both serpentinite and metacumulate have harzburgite protoliths (*cf.* [53]; Fig. 5).

Talc-bearing rocks from the Novillo and Peregrina Canyons have MgO of 26–33 wt%, SiO_2 of 43–61 wt%, FeO of 3.7–6.5 wt%, Al_2O_3 of < 1.2 wt% and CaO of < 2.0 wt%, whereas the talc from the Aramberri Uplift has MgO of 26 wt%, SiO_2 of 31 wt%, FeO of 9.8 wt%, Al_2O_3 of 19 wt% and CaO of 0.25 wt%. The Mg# in both areas is similar with values from 83 to 93.

4.2.2 Trace-element composition

The metacumulate and serpentinite rocks have high Cr concentrations of 96–5500 ppm, Ni of 100–4000 ppm and Co of 11–26 ppm. Ni/Co ranges between 11 and 26. The talc-bearing rocks from the Novillo and Peregrina Canyons have lower Cr concentrations of 82–2300 ppm, Ni of 160–1300 ppm, higher Co of 27–61 ppm and Ni/Co of 5–98. The talc-bearing rocks from the Aramberri Uplift have similar concentrations of Cr of 14–1900 ppm, Ni of 230–2100 ppm, Co of 19–93 ppm and Ni/Co ratio of 12–22. This composition suggests a depleted-mantle source (*cf.* [54]).

The incompatible elements for the Peregrina and Novillo Canyon meta-ultramafic rocks have highly scattered primitive mantle normalized values ($\text{Sr} = 1$ –184 ppm, $\text{Ba} = 1$ –15 ppm, $\text{K} = 0.01$ –0.04 ppm, $\text{Cs} = 0.1$ –280 ppm, $\text{U} = 0.1$ –0.2 ppm, $\text{Pb} = 0.1$ –14 ppm, $\text{Zr} = 0.1$ –60 ppm and $\text{Ce} = 0.1$ –1.9 ppm; Figs. 6a, b and c). The talc-bearing rocks of the Aramberri Uplift have similar incompatible elements patterns with $\text{K} = 0.01$ –0.04, $\text{Sr} = 8.70$ ppm, $\text{Cs} = 0.1$ ppm, $\text{U} = 2.8$ ppm, $\text{Pb} = 1.3$ ppm, $\text{Zr} = 2.2$ ppm (Fig. 6a).

The talc-bearing rocks from the Aramberri Uplift are enriched in light REE with La_N/Yb_N of 20 and low La_N/Sm_N ratio of 5.4 (N = Normalized values after [54]; Fig. 6d). The serpentinite rocks in the Peregrina and Novillo Canyon show two different patterns a) flat REE patterns with La_N/Yb_N ratio of 0.51–2.87 and La_N/Sm_N ratio of 0.72–2.58 (Figs. 6e and f) and b) slightly enriched REE patterns with La_N/Yb_N ratio of 9–10 and La_N/Sm_N ratio of 2–10. The talc-bearing rocks from the Peregrina and Novillo canyons have similar patterns to the serpentinite with La_N/Yb_N values of 0.60–1.5 and La_N/Sm_N values of 0.59–1.3 (Fig. 6d). These REE patterns suggest an abyssal peridotite source (MOR-type; *cf.* [55]).

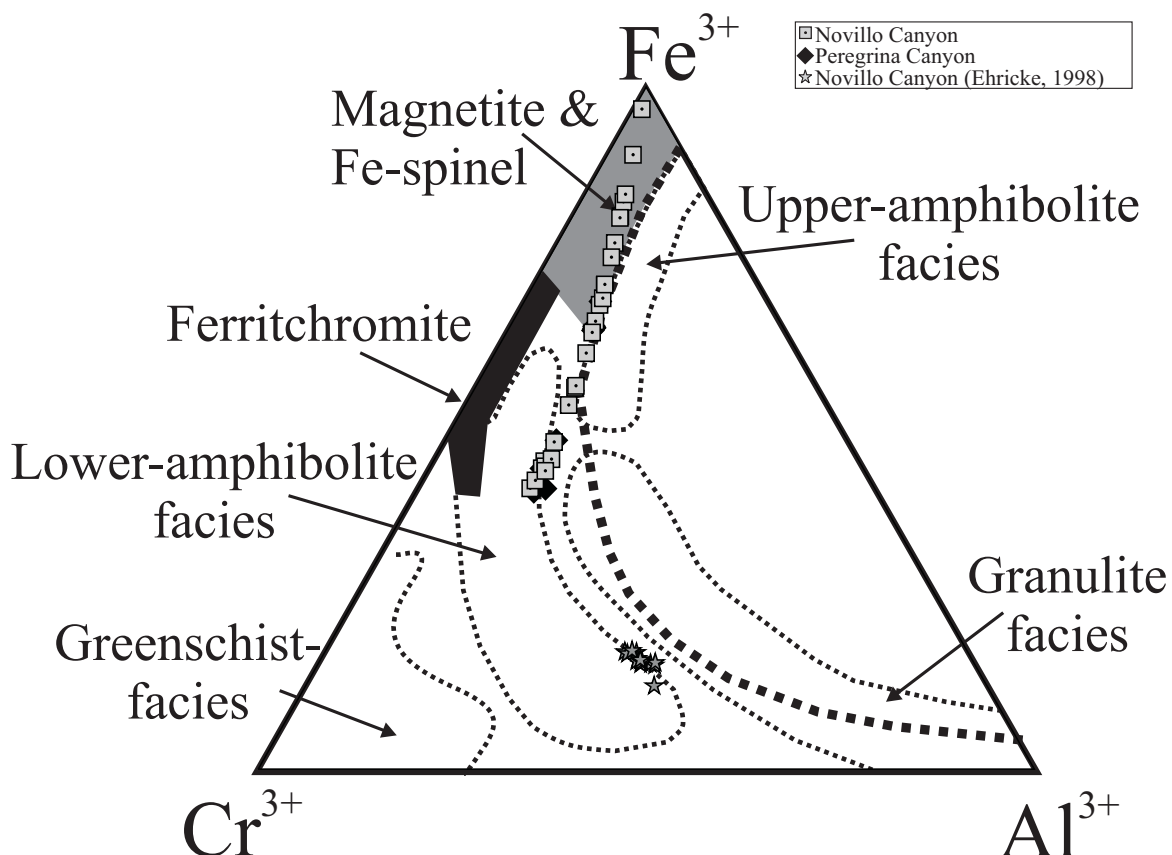


Figure 4: Ternary diagram of atomic Cr^{3+} - Fe^{3+} - Al^{3+} . Discrimination fields after [52].

5 Discussion

The chromite composition indicates an origin for the ultramafic rock protoliths in a mid-oceanic ridge setting. This is based on the Cr# and Mg# values of the Al-chromite in the serpentinite rocks from the Novillo and Peregrina canyons. The low Al^{3+} , Cr^{3+} , Fe^{3+} and TiO_2 contents in the Al-chromite is comparable to podiform (ophiolitic) and abyssal peridotite chromite (*cf.* [50, 56–59]; Fig. 7a–c). Al-chromite suggest that the Cr-spinel crystallized through high degrees of partial melting at the shallowest levels of an upper mantle source (within the Moho Transition Zone), i.e., close to the layered gabbro sequence (*e.g.* [60–65]).

Trace element enrichment of Cs, Rb, Pb, Sb, Sr are caused due serpentinization process, tremolite and/or carbonate precipitation also caused Pb, Sb enrichment and produces in serpentinites (*cf.* [66]) REE patterns are similar to fore-arc and mid-ocean-ridge serpentinites (*cf.* [66]) suggesting this environment for the serpentinization process.

The serpentinization of the peridotitic rocks occurred in two tectonic settings: (1) during ocean-floor metamorphism at a mid-ocean ridge and (2) through dynamic metamorphism at a subduction zone (*cf.* [60]; Fig. 7c).

Ocean-floor metamorphism produced mobility of trace elements as Rb and Sr, enrichment of Pb, Sb by carbonate precipitation and U-enrichment due hydrothermal alteration (*cf.* [66, 67]), pseudomorphic replacement textures, such as mesh texture (chrysotile and lizardite) and bastite were also formed. The presence of grossular in the metacumulate rock from the Novillo Canyon indicates rodingitization. According to [68] rodingite formation takes place at 200–300°C during ocean-floor metamorphism of ultramafic rocks (*cf.* [69, 70]). All this suggests that the first serpentinization took place under sub-greenschist to lower greenschist facies conditions, in accordance with the estimated temperatures of 253–293°C, while the rocks were located close to an oceanic spreading center (Fig. 8).

However, the slightly enrichment of LREE and Cs-enrichment in some serpentinites samples and the formation of ferrian chromite rims, box work textures, veins and

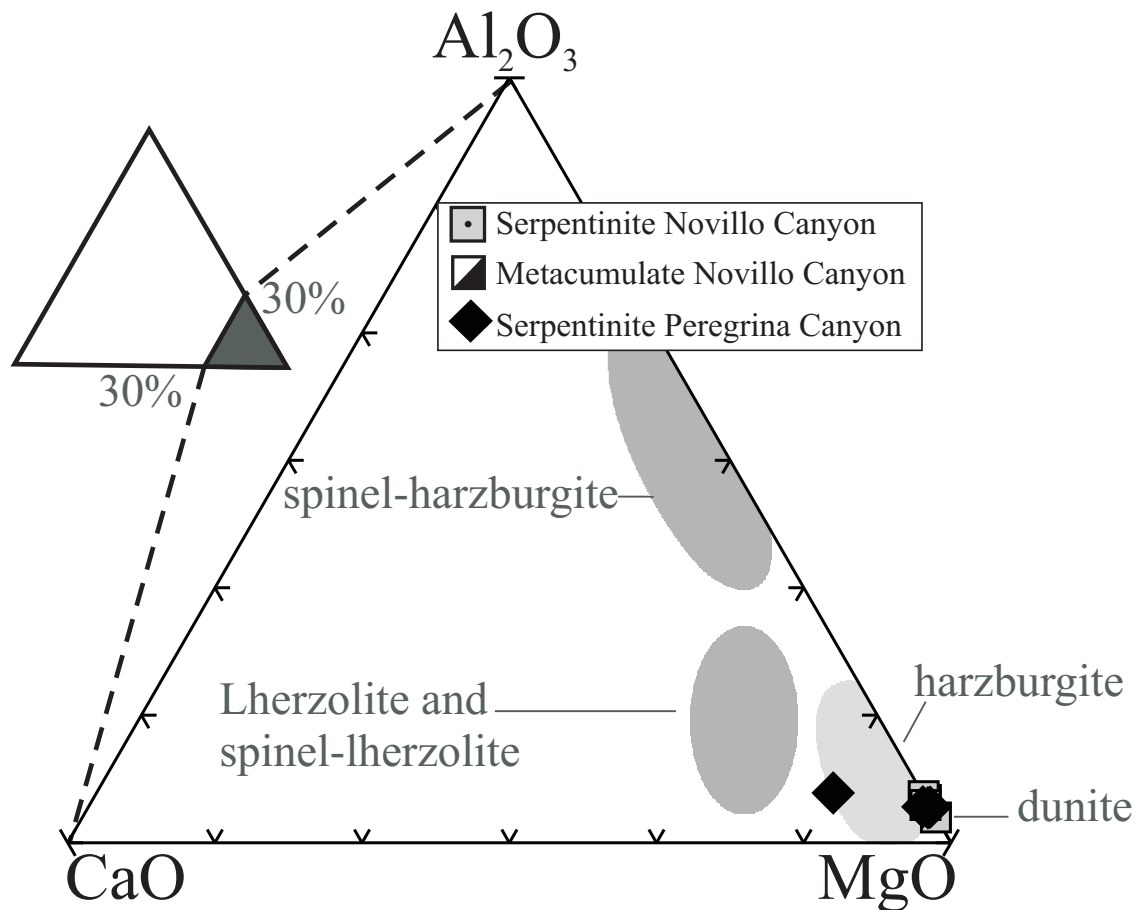


Figure 5: Relationship between serpentinite and its protoliths. Compositions are in mole%. After [53].

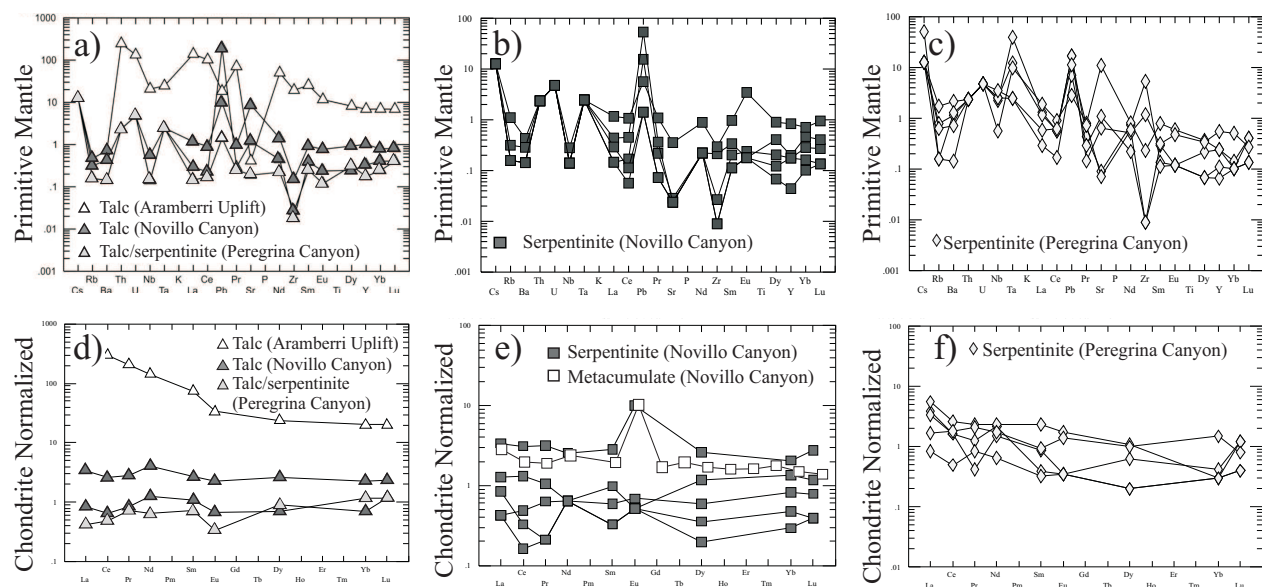


Figure 6: Primitive mantle-normalized trace element and chondrite-normalized rare earth element abundances in the meta-ultramafic rocks. Normalizing values after [54].

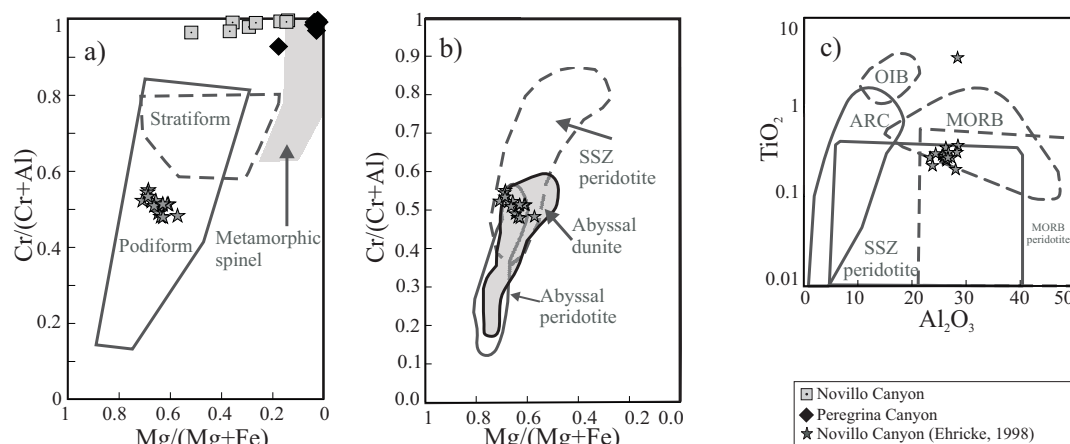


Figure 7: Chromite composition. a) Primary Mg/(Mg+Fe) and Cr/(Cr+Al) after [56, 57], b) after [50], c) Al₂O₃ vs. TiO₂ after [59], ARC =arc basalt; MORB: mid-ocean ridge basalt, OIB: ocean-island basalt, SSZ: suprasubduction zone.

Pennsylvanian-Permian (300 Ma)

(Northwest Gondwana)

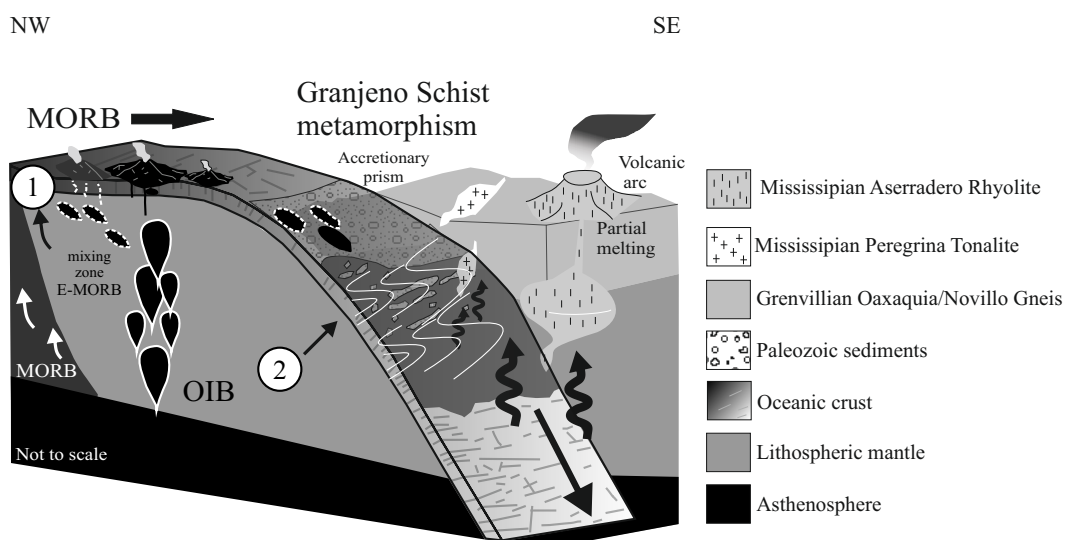


Figure 8: Serpentization model for the ultramafic rocks of the Granjeno Schist. 1: First serpentization in a mid-ocean ridge, Al-chromite formation, 2: main serpentization in a subduction zone, Fe-chromite and magnetite formation, MORB: mid-ocean ridge basalt, Mag: magnetite, SGSF: sub-greenschist facies, GSF: greenschist facies, LAF: Low amphibole facies.

ribbons of antigorite indicates a higher serpentinization degree, probably during the onset of regional metamorphism (Fig. 8). During this process the formation of chlorite rims, progressive replacement of Al-rich spinel by ferrian chromite and magnetite occurred. However, the association of ferrian chromite, antigorite, talc, tremolite and diopside indicates serpentinization at amphibolite facies (*cf.* [71–74]). This is supported by the occurrence of the minor phase pentlandite indicates recrystallization of pri-

mary sulfides at temperatures around 450°C during serpentinization (*cf.* [49]).

The related fault contact of the talc-bearing rock bodies with metasedimentary rocks, the formation of interpenetrative antigorite in serpentine, the replacement of serpentine crystals by talc and the appearance of calcite in veins and groundmass indicate a later crystallization stage for the Aramberri Uplift rocks. This suggests that a process

of obduction of the meta-ultramafic rocks related with regional metamorphism may have occurred.

5.1 Correlation of the meta-ultramafic rocks with metavolcanic and metasedimentary rocks in the Granjeno Schist

Serpentinite rocks record the evolution of seafloor formation affected at least for two metamorphic events at an ocean ridge and a later secondary metamorphism in a subduction zone. Neither indication for geochemical involvement of continental crust nor for subduction magmatism in the ultramafic protoliths, and due to the presence of associated oceanic basalts, we suggest that the magmatic evolution was completely within an oceanic plate.

Depositional contacts of clastic (continental) metasedimentary rocks with metavolcanic rocks throughout the Granjeno Schist suggest that sedimentation was contemporaneous with the volcanism. The age of the basaltic rocks remain unknown, but maximum depositional ages of the coeval metasedimentary rocks are late Cambrian to Devonian [18, 75], indicating a composite unit with a long possible sedimentation and volcanism history. Grenvillian (1250–920 Ma) and Panafrican (730–530 Ma) detrital zircon crystallization ages suggest that the Novillo Gneiss of the Oaxaquia microcontinent and the Gondwana continent may have been the main sediment sources [18, 75]. Thus, the Granjeno Schist can be related to the Rheic Ocean.

Assuming that the youngest maximum depositional ages are similar to the youngest depositional part of the Granjeno Schist, N-MORB igneous activity and sedimentation in the Novillo and Peregrina Canyon area lasted at least from Silurian to Devonian times [19]. The extrusion of N-MORB from asthenospheric magma can be related to rifting and drifting of part of the Rheic Ocean during that time. The abyssal peridotite (meta-ultramafic rocks) may have formed in this scenario. The peridotite represents the melting residues of N-MORB melt. It became exposed on the seafloor due to tectonic faulting associated with spreading-ridge extension. During the spreading of the ocean floor alteration, low-grade metamorphism, initial serpentinization and rodginization took place.

Regional studies about southern and northeastern Mexico indicate that the closure of the Rheic Ocean did not result in a subsequent continent-continent collision, but moved Gondwana into contact with the Paleo-Pacific Ocean (e.g., [14, 20, 76]). As result dextral transpression took place and a Pennsylvanian-Permian magmatic arc was established (*cf.* [14, 15, 18, 77, 78]). The metamorphic

age of the Granjeno Schist indicates that the metamorphic overprint and the second serpentinization event of the rocks of the present study may have taken place in an accretionary prism during Pennsylvanian to Permian times (*cf.* [18]).

The low-metamorphic conditions for the Granjeno Schist are untypical for a continent-continent collision. Instead, accretion and obduction in an evolving active margin is more plausible [19]. This is in accordance with the metamorphic age of the Granjeno Schist as well as with the presence of plagiogranite with syn-collisional and volcanic-arc characteristics, which intruded the Novillo Gneiss at c. 350 Ma [13, 79]. During the obduction and accretion at the active margin, talc formed through thrust faulting of serpentinized ultramafic rocks, with metavolcanic and metasedimentary rocks (*cf.* [80–82]).

6 Conclusions

The presented data suggest that the serpentinites and associated rocks represent a fragment of oceanic lithosphere that was formed and modified during the propagation of the ocean floor. Serpentinization presumably took place from a depleted-mantle source at the Moho Transition Zone up to the layered gabbro level. The process occurred over extended time and temperature ranges at sub-greenschist to greenschist facies metamorphic conditions. After the ocean-floor serpentinization, a second regional-metamorphic serpentinization phase took place during this event the lithospheric mantle slivers juxtaposed in the forearc region. These geological processes are related to a proposed circum-Pangaea non-collisional subduction zone, which caused prograde metamorphism in northeastern Mexico at Pennsylvanian to Permian time during Pangaea configuration.

Acknowledgement: The field work was supported by the project PaicyT and the Facultad de Ciencias de la Tierra, Universidad Autónoma de Nuevo León (UANL), México. The geochemical analyses were supported by Dr. Jenchen. Microprobe analyses were funded by the Institute of Geosciences of the Friedrich-Schiller University Jena, Germany (FSU), by the Best Thesis Award 2010 granted by UANL and Dr. Ramírez-Fernández. Acknowledgement to the support from ConacyT for a research stay at the Institute of Geosciences, FSU, during 2012 financed by the Scholarship “Becas Mixtas 2012-2013 Movilidad en el extranjero” with scholarship number 239341 and DAAD for the “Research

Grant for Doctoral Candidates and Young Academics and Scientist 2013-2015" scholarship number 57076385.

References

- [1] Mickus, K., Montana, C., Crustal structure of northeastern Mexico revealed through the analysis of gravity data. In: Mesozoic sedimentary and tectonic history of north-central Mexico, C. Bartolini, J. Wilson and T. Lawton, (eds.). Geological Society of America, Special Paper Boulder Colorado, 1999, 340, 357-372.
- [2] Carrillo-Bravo, J., Geología del Anticlinorio Huizachal-Peregrina al NW de Ciudad Victoria, Tamaulipas. Boletín de la Asociación Mexicana de Geólogos Petroleros 1961, 13,1-98
- [3] De Cserna, Z., Ortega-Gutiérrez, F., Alóctono del Paleozoico inferior en la región de Ciudad Victoria, estado de Tamaulipas. Revista del Instituto de Geología de la Universidad Nacional Autónoma de México, 1977, 1, 33-43.
- [4] Ramírez-Ramírez, C., Reinterpretación tectónica del Esquisto Granjeno de Ciudad Victoria, Tamaulipas. MSc. Thesis. Universidad Nacional Autónoma de México, Facultad de Ingeniería, 1978.
- [5] Castillo-Rodríguez, H., Zur Geologie des kristallinen Grundgebirges der Sierra Madre Oriental – insbesondere des Granjeno-Schiefer-Komplexes im Südteil des Huizachal-Peregrina-Antiklinoriums (Raum Ciudad Victoria, Tamaulipas, Mexiko). MSc. Thesis, University of Münster, 1988.
- [6] Cossío-Torres, T., Zur Geologie der Sierra Madre Oriental – insbesondere des Novillo-Gneis-Komplexes - im Südteil des Huizachal-Peregrina-Antiklinoriums (Raum Ciudad Victoria, Tamaulipas, Mexiko). MSc. Thesis, University of Münster, 99, 1988.
- [7] Orozco-Equivel, M.T., Zur Petrologie des Kristallins im Huizachal-Peregrina- Fenster, Sierra Madre Oriental Mexiko. Diploma Thesis, University of Karlsruhe, 1991.
- [8] Ramírez-Ramírez, C., Pre-Mesozoic geology of Huizachal-Peregrina anticlinorium, Ciudad Victoria, Tamaulipas, and adjacent parts of eastern México. Ph.D Thesis, University of Texas, Austin, 1992.
- [9] Ortega-Gutiérrez, F., Ruiz, J., Centeno-García, E., Oaxaquia, a Proterozoic microcontinent accreted to North America during the late Paleozoic. *Geology*, 1995, 23, 12, 1127-1130.
- [10] Ehrcke, C., Mafische und ultramafische Gesteine des Novillo-Canyons, Sierra Madre Oriental, Mexiko. Institut für Mineralogie, Petrologie und Geochemie der Albert-Ludwigs-Universität Freiburg, Diploma Thesis, 1998.
- [11] Torres-Sánchez, S.A., Petrología e Interpretación Geodinámica del Esquisto Granjeno en el Cañón de Caballeros, Anticlinorio Huizachal-Peregrina, NE de México. Bachelor thesis, Universidad Autónoma de Nuevo León, 2010
- [12] Keppie, J.D., Ortega-Gutiérrez, F., Middle American Precambrian basement: a missing piece of the reconstructed 1 Ga orogen. In: Ramos, V.A., Keppie, J.D. (eds.). Laurentia-Gondwana connections before Pangea. Geological Society of America Special Paper, 1999, 336, 199–210.
- [13] Dowe, D. S., Nance, R. D., Keppie, J. D., Cameron, K. L., Ortega-Rivera, A., Ortega-Gutiérrez, F., Lee, J. W. K., Deformational history of the Granjeno Schist, Ciudad Victoria, Mexico: Constraints on the closure of the Rheic Ocean? *International Geology Review*, 2005, 47, 9, 920-937.
- [14] Nance, R. D., Miller, B. V., Keppie, J. D., Murphy, J. B., Dostal, J., Vestige of the Rheic Ocean in North America: the Acatlán Complex of southern México. *Special Papers Geological Society of America*, 2007, 423, 437.
- [15] Nance, R. D., Linnemann, U., The Rheic Ocean: origin, evolution, and significance. *GSA Today*, 2008, 18, 12, 4-12.
- [16] Nance, R. D., Keppie, J. D., Miller, B. V., Murphy, J. B., Dostal, J., Palaeozoic palaeogeography of Mexico: constraints from detrital zircon age data. *Geological Society of London, Special Publications*, 2009, 327, 1, 239-269.
- [17] Nance, R.D., Gutiérrez-Alonso, G., Keppie, J.D., Linnemann, U., Murphy, J.B., Quesada, C., Strachan, R.A., Woodcock, N., Evolution of the Rheic Ocean. *Gondwana Research*, 2010, 17, 2-3, 194-222.
- [18] Barboza-Gudiño, J. R., Ramírez-Fernández, J. A., Torres-Sánchez, S. A., Valencia, V. A., Geocronología de circones detriticos de diferentes localidades del Esquisto Granjeno en el noreste de México. *Boletín de la Sociedad Geológica Mexicana*, 2011, 63, 2, 201-216.
- [19] Torres Sánchez, S. A., Augustsson, C., Barboza Gudiño, J. R., Jenchen, U., Ramírez Fernández, J. A., Abratis, M., Scherstén, A Magmatic source and metamorphic grade of metavolcanic rocks from the Granjeno Schist: was northeastern Mexico a part of Pangaea? *Geological Journal*, 2015, 51, 845-863.
- [20] Unrug, R., The supercontinent cycle and Gondwanaland assembly: component cratons and the timing of suturing events. *Journal of Geodynamics*, 1992, 16, 4, 215-240.
- [21] Keppie, J. D., Dostal, J., Murphy, J. B., Nance, R. D., Synthesis and tectonic interpretation of the westernmost Paleozoic Variscan orogen in southern Mexico: From rifted Rheic margin to active Pacific margin. *Tectonophysics*, 2008, 461, 1, 277-290.
- [22] Keppie, J. D., Nance, R. D., Ramos-Arias, M. A., Lee, J. K. W., Dostal, J., Ortega-Rivera, A., Murphy, J. B., Late Paleozoic subduction and exhumation of Cambro-Ordovician passive margin and arc rocks in the northern Acatlán Complex, southern Mexico: Geochronological constraints. *Tectonophysics*, 2010, 495, 3, 213-229.
- [23] Keppie, J. D., Ramos, V.A.R., Odyssey of terranes in the Iapetus and Rheic oceans during the Precambrian. In: Laurentia Gondwana Connections before Pangea, Ramos, V.A., Keppie, J.D. (eds.). Geological Society of America Special Paper, 1999, 336: Boulder Colorado 267-275.
- [24] Keppie, J. D., Terranes of Mexico revisited: A 1.3 billion year odyssey. *International Geology Review*, 2004, 46, 9, 765-794.
- [25] Nance, R. D., Murphy, J. B., Strachan, R. A., Keppie, J. D., Gutiérrez-Alonso, G., Fernández-Suárez, J., Pisarevsky, S. A., Neoproterozoic-early Palaeozoic tectonostratigraphy and palaeogeography of the peri-Gondwanan terranes: Amazonian v. West African connections. *Geological Society, London, Special Publications*, 2008, 297, 1, 345-383.
- [26] Denison, R.E., Burke, W.H., Jr., Hetherington, Otto, J.B., Basement rock framework of parts of Texas, southern New Mexico and northern Mexico. In: The Geologic framework of the Chihuahua Tectonic Belt: Midland, Texas, Seewald, K. Sundeen, D. (eds.). *West Texas Geological Society Publications*, 1971, 3-14.
- [27] Garrison, J.R., Jr., Ramirez-Ramirez, C., Long, L.E., Rb-Sr isotopic study of the ages and provenance of Precambrian granulite and Paleozoic greenschist near Ciudad Victoria, Mexico. In: Pilger,

- R.H., Jr., (ed.). Symposium on the origin of the Gulf of Mexico and the early opening of the central north Atlantic ocean, Louisiana State University, Baton Rouge, 1980, 37-49.
- [28] Ortega-Gutiérrez, F., El Gneis Novillo y rocas metamórficas asociadas en los Cañones del Novillo y de la Peregrina, área de Ciudad Victoria, Tamaulipas. *Revista del Instituto de Geología, Universidad Nacional Autónoma de México*, 1978, 2, 1, 19-30.
- [29] Dowe, D. S., Deformational History of the Granjeno Schist Near Ciudad Victoria, Mexico, PhD Thesis, Ohio University, 2004.
- [30] Alemán-Gallardo, E., Remanentes del piso oceánico en la secuencia paleozoica metamorfizada de la margen NW de Gondwana en el estado de Tamaulipas, NE de México: Serpentinita Victoria. Universidad Autónoma de Nuevo León, Bachelor Thesis, 2013.
- [31] Scotese, C.R., Langford, R., Pangea and the Paleogeography of the Permian. In: P.A. Scholle, T. M. Peryt, and D. S. Ilmer-Scholle, (Eds.) *The Permian of Northern Pangea 1*, Springer-Verlag, Berlin, 1995, 3-19.
- [32] Cawood, P. A., Kröner, A., Collins, W. J., Kusky, T. M., Mooney, W. D., Windley, B. F., Accretionary orogens through Earth history. Geological Society, London, Special Publications, 2009, 318, 1-36.
- [33] Ziegler, P.A., Geological Atlas of Western and Central Europe. In: Shell Internationale Petroleum Maatschappij BV, The Hague, Belgium, 2nd Ed., Geological Society of London, 1990, 239.
- [34] Stampfli, G.M., Borel, G.D., A plate tectonic model for the Paleozoic and Mesozoic constrained by dynamic plate boundaries and restored synthetic ocean isochrons. *Earth and Planetary Science Letters*, 2002, 196, 17-33.
- [35] Blakey, R.C., Carboniferous-Permian paleogeography of the assembly of Pangea. In Wong, T.E., (ed.). Fifteenth International Congress on Carboniferous and Permian Stratigraphy, Utrecht, the Netherlands, Royal Netherlands Academy of Arts and Sciences, 2007, 443-465.
- [36] Elías-Herrera, M., Ortega-Gutiérrez, F., Caltepec fault zone: An Early Permian dextral transpressional boundary between the Proterozoic Oaxacan and Paleozoic Acatlán complexes, southern Mexico, and regional tectonic implications. *Tectonics*, 2002, 21, 3, 4-1.
- [37] Keppe, J. D., Dostal, J., Miller, B. V., Ramos-Arias, M. A., Morales-Gámez, M., Nance, R. D., Cooper, P., Ordovician-earliest Silurian rift tholeiites in the Acatlán Complex, southern Mexico: Evidence of rifting on the southern margin of the Rheic Ocean. *Tectonophysics*, 2008, 461, 1, 130-156.
- [38] Zhou, Y., Murphy, M. A., Hamade, A., Structural development of the Peregrina-Huizachal anticlinorium, Mexico. *Journal of structural geology*, 2006, 28, 3, 494-507.
- [39] Imlay, R.W. Studies of the Mexican geosyncline. *Geological Society of America Bulletin*, 1938, 49, 11, 1651-1694.
- [40] Heim, A., The front ranges of Sierra Madre Oriental. Mexico, from Ciudad Victoria to Tamazunchale. *Ectogae Geologicae Helveticae*, 1940, 33, 2, 313-352.
- [41] Humphrey, W. E., Stratigraphy of the Cortinas Canyon Section, Sierra de los Muertos, Coahuila, Mexico. In Díaz, T., (ed.). 21st Field Trip Guide Book, South Texas Geological Society, 1954, 89-176.
- [42] Mixon, R.B., Murray, G.E., Diaz, T.G., Age and correlation of Huizachal Group (Mesozoic), State of Tamaulipas, Mexico. *Bulletin of American Association Petroleum Geologists*, 1959, 43, 757-771.
- [43] Barboza-Gudiño, J. R., Gómez-Anguiano, M., Zavala-Monsiváis, A., The Early Mesozoic volcanic arc of western North America in northeastern Mexico. *Journal of South American Earth Sciences*, 2008, 25, 1, 49-63.
- [44] Fries, C., Schmitter, E., Damon, P.E., Livingston, D.E., Erickson, R., Edad de las rocas metamórficas de los cañones de la Peregrina y de Caballeros parte centro-occidental de Tamaulipas. *Boletín del Instituto de Geología*, 1962, 64, 55-69.
- [45] De Cséna, Z., Ortega-Gutiérrez, F., Reinterpretation of isotopic age data from the Granjeno Schist, Ciudad Victoria, Tamaulipas. *Revista Mexicana de Geociencias de la Universidad Nacional Autónoma de México*, 1978, 2, 31-36.
- [46] Sedlock, R. L., Ortega-Gutiérrez, F., Speed, R. C., Tectonostratigraphic terranes and tectonic evolution of Mexico. *Geological Society of America Special Papers*, 1993, 278, 1-153.
- [47] Cathelineau, M., Cation site occupancy in chlorites and illites as a function of temperature. *Clay Minerals*, 1988, 23, 471-485.
- [48] Jowett, E. C., Fitting iron and magnesium into the hydrothermal chlorite geothermometer. In: GAC/MAC/SEG, Joint Annual Meeting Program with Abstracts, 1991, 16, A-62.
- [49] Deer, W.A., Howie, R.A., Zussman, J., An introduction to the rock forming minerals, Longman Scientific and Technical 2nd ed., London, 2013..
- [50] Dick, H.J.B., Bullen, T., Chromian spinel as a petrogenetic indicator in abyssal and alpine-type peridotites and spatially associated lavas. *Contributions to Mineralogy and Petrology*, 1984, 86, 54-76.
- [51] Aswad, K. J., Aziz, N. R., Koyi, H. A., Cr-spinel compositions in serpentinites and their implications for the petrotectonic history of the Zagros Suture Zone, Kurdistan Region, Iraq. *Geological Magazine*, 2011, 148, 5-6, 802-818.
- [52] Saumur, B. M., & Hattori, K. H., Zoned Cr-spinel in forearc serpentinites along the northern Caribbean Margin, Dominican Republic. *Mineralogical Magazine*, 2013, 77, 117-136.
- [53] Li, X.P., Rahn, M., Bucherker., Serpentinization of the Zermatt-Saas, ophiolite complex and their texture evolution: *Journal of Metamorphic Geology*, 2004, 22, 159 - 177.
- [54] Azer, M. K., Khalil, A. E. S., Petrological and mineralogical studies of Pan-African serpentinites at Bir Al-Edeid area, central Eastern Desert, Egypt. *Journal of African Earth Sciences*, 2005, 43, 5, 525-536.
- [55] Sun, S.S., McDonough, W.F., Chemical and isotopic systematics of oceanic basalts: implications for mantle compositions and processes. In: Saunders, A.D., Norry, M.J. (Eds.), *Magmatism in the Ocean Basins*. Geological Society Special Publication, 1989, 42, 1, 313-345.
- [56] Niu, Y., O'Hara, M. J., Origin of ocean island basalts: A new perspective from petrology, geochemistry, and mineral physics considerations. *Journal of Geophysical Research: Solid Earth*, 2003, 108, 1978-2012.
- [57] Irvine, T.N., Chromian spinel as a petrogenetic indicator: petrologic applications. *Canadian Journal of Earth Sciences*, 1967, 4, 71-103.
- [58] Leblanc, M., Nicolas, A., Les chromitites ophiolitiques. *Chronique de la Recherche Minière*, 1992, 507, 3-25.
- [59] Nicolas, A., Structures of ophiolites and dynamics of ocean lithosphere: Petrology and structural geology. Kluwer Academic Publishers, Amsterdam, 1989.
- [60] Kamenetsky, V., Crawford, A.J., Meffre, S., Factors controlling chemistry of magmatic spinel: an empirical study of associated

- olivine, Cr-spinel and melt inclusions from primitive rocks. *Journal of Petrology*, 2001, 42, 655–671.
- [61] Arai, S., Yurimoto, H., Possible sub-arc origin of podiform chromitites. *Island Arc*, 1995, 4, 2, 104-111.
- [62] Zhou, X.H., Sun, M., Wilde, S., “In-situ” comparative study on granulite xenoliths vs. granulite terrains in Hannuoba region, North China: isotopic constrains Chinese *Science Bulletin*, 1998, 43, 164.
- [63] Proenza, J., Gervilla, F., Melgarejo, J., Bodinier, J. L., Al-and Cr-rich chromitites from the Mayarí-Baracoa ophiolitic belt (eastern Cuba); consequence of interaction between volatile-rich melts and peridotites in suprasubduction mantle. *Economic Geology*, 1999, 94, 4, 547-566.
- [64] Proenza, J. A., Ortega-Gutiérrez, F., Camprubí, A., Tritlla, J., Elias-Herrera, M., Reyes-Salas, M., Paleozoic serpentinite-enclosed chromitites from Tehuitzingo (Acatlán Complex, southern Mexico): a petrological and mineralogical study. *Journal of South American Earth Sciences*, 2004, 16, 8, 649-666.
- [65] Proenza, J. A., Zaccarini, F., Escayola, M., Cábana, C., Schalamuk, A., Garuti, G., Composition and textures of chromite and platinum-group minerals in chromitites of the western ophiolitic belt from Pampean Ranges of Córdoba, Argentina. *Ore Geology Reviews*, 2008, 33, 1, 32-48.
- [66] Kodolányi, J., Pettke, T., Spandler, C., Kamber, B. S., Gméling, K., Geochemistry of ocean floor and fore-arc serpentinites: constraints on the ultramafic input to subduction zones. *Journal of Petrology*, 2011, 53, 2, 235-270.
- [67] Humphriss, S. E., Thompson, G., Trace element mobility during hydrothermal alteration of oceanic basalts. *Geochimica et Cosmochimica Acta*, 1978, 42, 1, 127-136.
- [68] O’Hanley, D. S., Schandl, E. S., & Wicks, F. J., The origin of rodingites from Cassiar, British Columbia, and their use to estimate T and P (H_2O) during serpentinization. *Geochimica et Cosmochimica Acta*, 1992, 56, 1, 97-108.
- [69] Hernández, L., Barra, F., Hidrogrosularia-uvaroitas, vesuvianita y perovskita: productos de rodingitización de rocas ultramáficas del área de La Cabaña, IX Región, Chile. In *Congreso Geológico Chileno*, 1997, 8, 1309-1313.
- [70] Bucher, K., Grapes, R., *Petrogenesis of Metamorphic Rocks*. Springer Berlin-Heidelberg, 2011.
- [71] Springer, R.K., Contact metamorphosed ultramafic rocks in the Western Sierra Nevada foothills, California. *Journal of Petrology*, 1974, 15, 160-195.
- [72] Ashley, P. M., Opaque mineral assemblage formed during serpentinization in the Coolac ultramafic belt, New South Wales. *Journal of the Geological Society of Australia*, 1975, 22, 91-102.
- [73] Bliss, N. W., MacLean, W. H., The paragenesis of zoned chromite from central Manitoba. *Geochimica et Cosmochimica Acta*, 1975, 39, 6, 973-990.
- [74] Evans, B.W., Frost, B.R., Chrome-spinel in progressive metamorphism a preliminary analysis. *Geochimica et Cosmochimica Acta*, 1975, 39, 959-972.
- [75] Torres-Sánchez, S. A., Augustsson, C., Ramírez Fernández, J.A., Barboza Gudiño, J. R., Jenchen, U., Abratis, M., Geochemistry and metamorphism of the Paleozoic metasedimentary basement of the Sierra Madre Oriental, NE Mexico. Possible paths from their depositional environment?. In: *Geological Society of America Program with Abstracts*, 2013, 45, 3, A-60.
- [76] Dickinson, W. R., Lawton, T. F., Carboniferous to Cretaceous assembly and fragmentation of Mexico, *Geological Society of America Bulletin*, 2001, 113, 9, 1142-1160.
- [77] Keppie, J. D., Nance, R. D., Dostal, J., Lee, J. K. W., Ortega-Rivera, A., Constraints on the subduction erosion/extrusion cycle in the Paleozoic Acatlán Complex of southern Mexico: geochemistry and geochronology of the type Piaxtla Suite. *Gondwana Research*, 2012, 21, 4, 1050-1065.
- [78] Nance, R. D., Gutiérrez-Alonso, G., Keppie, J. D., Linnemann, U., Murphy, J. B., Quesada, C., Woodcock, N. H., A brief history of the Rheic Ocean. *Geoscience Frontiers*, 2012, 3, 2, 125-135.
- [79] De-León-Barragán, L., Magmatismo ácido en el Basamento de la Sierra Madre Oriental, Anticlinorio Huizachal - Peregrina, Tamaulipas, México. Bachelor Thesis, Universidad Autónoma de Nuevo León, 2012.
- [80] Beaulieu P., Les gisements de talc du Val Malenco (Italie du Nord). *Chronique de la Recherche Minière*, 1985, 478, 5-20.
- [81] Salem I.A., Talc deposits at Rod El-Tom and Umm El-Dalalil areas, Eastern Desert, Egypt. *Egypt Journal of Geology*, 1992, 36, 1-2, 175-189.
- [82] Karlsen T.A., Rian E. and Olesen O, Overview of talc resources in the Altermark talc province, northern Norway, and possible uses of the talc ore. *NGU Bulletin*, 2000, 436, 93-102.

Appendices

Appendix 1 Serpentine microprobe data and structural formulae based on 14 oxygen

Appendix 1. Serpentine microprobe data and structural formulae based on 14 oxygen.											
Sample	MS10_1	MS10_5	MS10_7	MS10_30	MS6_1	MS6_2	MS6_40	MS10_41	MT6_1	MT6_7	MT6_15
SiO ₂	42.35	42.48	39.53	41.99	36.74	37.32	44.65	42.82	30.98	30.26	30.97
TiO ₂	0.01	0.01	0.01	0.00	0.04	0.03	0.02	0.01	0.01	0.00	0.00
Al ₂ O ₃	1.27	1.32	2.92	1.59	4.77	4.30	0.72	1.15	13.88	15.82	15.00
Cr ₂ O ₃	0.14	0.14	1.20	0.29	1.99	2.00	0.13	0.32	5.04	2.14	2.86
FeO	6.08	6.38	7.05	6.69	4.05	4.03	1.65	6.42	10.96	11.32	11.17
MnO	0.05	0.05	0.03	0.05	0.01	0.01	0.05	0.06	0.13	0.13	0.11
MgO	37.33	36.85	35.59	36.67	37.70	37.57	38.16	36.24	25.91	26.26	25.63
CaO	0.07	0.04	0.01	0.42	0.03	0.02	0.06	0.00	0.03	0.07	0.14
Na ₂ O	0.00	0.01	0.00	0.00	0.02	0.03	0.11	0.00	0.01	0.01	0.03
K ₂ O	0.01	0.03	0.01	0.00	0.00	0.02	0.10	0.00	0.00	0.03	0.02
H ₂ O	12.69	12.70	13.65	12.29	14.65	14.68	14.34	12.99	13.05	13.96	14.07
Total oxide %	87.31	87.30	86.35	87.71	85.35	85.32	85.66	87.01	86.95	86.04	85.93
Si	4.01	4.02	3.83	3.97	3.57	3.63	4.19	4.06	3.09	3.03	3.10
Al	0.14	0.15	0.33	0.18	0.55	0.49	0.08	0.13	1.63	1.87	1.77
Ti	0.00	0.00	0.00	0.00	0.00	0.00	0.00	0.00	0.00	0.00	0.00
Cr	0.01	0.01	0.09	0.02	0.15	0.15	0.01	0.02	0.40	0.17	0.23
Mg	5.26	5.20	5.14	5.17	5.46	5.44	5.33	5.13	3.85	3.92	3.83
Fe	0.48	0.51	0.57	0.53	0.33	0.33	0.13	0.51	0.91	0.95	0.94
Mn	0.00	0.00	0.00	0.00	0.00	0.00	0.00	0.00	0.01	0.01	0.01
Ni	0.00	0.00	0.00	0.00	0.00	0.00	0.00	0.00	0.00	0.00	0.00
Ca	0.01	0.00	0.00	0.04	0.00	0.00	0.01	0.00	0.00	0.01	0.01
Na	0.00	0.00	0.00	0.00	0.00	0.00	0.02	0.00	0.00	0.00	0.01
K	0.00	0.00	0.00	0.00	0.00	0.00	0.01	0.00	0.00	0.00	0.00
Sum	9.92	9.90	9.96	9.93	10.08	10.05	9.78	9.86	9.90	9.96	9.90

Appendix 1. Serpentine microprobe data and structural formulae based on 14 oxygen.											
Mg#	91.63	91.15	90.00	90.72	94.32	94.32	97.63	80.82	80.59	80.06	90.96
Al _{tot}	0.27	0.28	0.63	0.34	1.03	0.93	0.15	0.25	3.11	3.55	3.38
Cr _{tot}	0.02	0.02	0.18	0.04	0.31	0.31	0.02	0.05	0.79	0.34	0.45
Fe _{tot}	0.48	0.51	0.57	0.53	0.33	0.33	0.13	0.51	0.91	0.95	0.94
Mg/Si	1.31	1.29	1.34	1.30	1.53	1.50	1.27	1.26	1.25	1.29	1.23

Appendix 2. Chlorite microprobe data and structural formulae based on 14 oxygen.												
Sample	MC1_33	MC1_37	MT5_17	MT5_18	MT5_19	MT5_20	MT5_22	MT5_23	MT5_24	MT5_28	MT5_29	MT5_30
SiO ₂	31.29	31.33	29.22	29.15	29.63	29.60	28.73	29.68	29.26	29.50	29.21	29.81
TiO ₂	0.02	0.00	0.00	0.01	0.05	0.04	0.03	0.03	0.03	0.00	0.02	0.02
Al ₂ O ₃	19.38	19.21	18.97	19.07	18.48	18.78	18.44	18.06	18.82	18.28	18.62	18.37
Cr ₂ O ₃	0.00	0.07	0.16	0.23	0.28	0.25	0.23	0.27	0.20	0.34	0.35	0.27
FeO	3.77	3.70	15.68	15.85	14.61	14.99	16.60	15.54	15.74	15.15	15.50	15.24
MnO	0.06	0.08	0.17	0.19	0.16	0.16	0.16	0.16	0.20	0.16	0.18	0.18
MgO	32.20	31.89	23.90	23.24	24.36	22.89	22.46	23.62	23.66	23.78	23.97	23.89
NiO	0.07	0.07	0.12	0.10	0.11	0.08	0.11	0.10	0.12	0.11	0.11	0.13
CaO	0.07	0.19	0.02	0.00	0.00	0.09	0.08	0.03	0.03	0.01	0.01	0.00
Na ₂ O	0.00	0.00	0.00	0.00	0.02	0.02	0.00	0.02	0.01	0.02	0.02	0.00
K ₂ O	0.01	0.00	0.01	0.01	0.03	0.02	0.02	0.13	0.01	0.04	0.03	0.04
Total Oxide %	86.87	86.54	88.26	87.85	87.73	86.92	86.87	87.65	88.07	87.38	88.02	87.95
Si	2.96	2.97	2.90	2.91	2.94	2.97	2.91	2.96	2.91	2.95	2.90	2.96
Al	2.16	2.15	2.22	2.24	2.16	2.22	2.20	2.13	2.21	2.15	2.18	2.15
Ti	0.00	0.00	0.00	0.00	0.00	0.00	0.00	0.00	0.00	0.00	0.00	0.00

Appendix 2 Chlorite microprobe data and structural formulae based on 14 oxygen

Appendix 2. Chlorite microprobe data and structural formulae based on 14 oxygen.											
Cr	0.00	0.01	0.01	0.02	0.02	0.02	0.02	0.02	0.02	0.03	0.03
Mg	4.53	4.51	3.53	3.45	3.60	3.42	3.40	3.52	3.51	3.54	3.55
Fe	0.30	0.29	1.30	1.32	1.21	1.26	1.41	1.30	1.31	1.27	1.29
Mn	0.00	0.01	0.01	0.02	0.01	0.01	0.01	0.01	0.02	0.01	0.01
Ni	0.01	0.01	0.01	0.01	0.01	0.01	0.01	0.01	0.01	0.01	0.01
Ca	0.01	0.02	0.00	0.00	0.00	0.01	0.01	0.00	0.00	0.00	0.00
Na	0.00	0.00	0.00	0.00	0.00	0.00	0.00	0.00	0.00	0.00	0.00
K	0.00	0.00	0.00	0.00	0.00	0.00	0.00	0.02	0.00	0.01	0.00
Sum	9.96	9.95	9.99	9.96	9.97	9.92	9.97	9.97	9.98	9.97	9.99
Al ^{IV}	1.04	1.03	1.10	1.09	1.06	1.03	1.09	1.04	1.09	1.05	1.10
Al ^{VI}	1.11	1.12	1.11	1.15	1.10	1.18	1.12	1.09	1.11	1.10	1.09
Al _{tot}	2.16	2.15	2.22	2.24	2.16	2.22	2.20	2.13	2.21	2.15	2.18
Fe/(Fe+Mg)	0.06	0.06	0.27	0.28	0.25	0.27	0.29	0.27	0.27	0.26	0.27
Mg/Mg+Fe	0.94	0.94	0.73	0.72	0.75	0.73	0.71	0.73	0.73	0.74	0.74
Si tot	7.70	7.75	7.54	7.57	7.66	7.75	7.59	7.72	7.57	7.68	7.56
T° Cathelineu, 1988	274	270	293	290	280	271	288	272	289	277	291

Appendix 3. Pyroxene microprobe data and structural formulae based on 6 oxygen.											
Sample	MC1_1	MC1_2	MC1_3	MC1_4	MC1_10	MC1_26	MC1_27	MC1_28	MC1_29	MC1_38	MC1_40
SiO ₂	53.56	53.21	55.05	54.62	54.35	54.37	54.75	55.29	53.88	56.16	55.46
TiO ₂	0.43	0.31	0.06	0.05	0.12	0.26	0.14	0.06	0.11	0.02	0.07
Al ₂ O ₃	1.73	2.95	0.88	0.33	1.10	1.07	0.78	0.50	0.52	0.17	0.65
Cr ₂ O ₃	0.34	0.35	0.23	0.13	0.20	0.33	0.10	0.14	0.13	0.05	0.11
FeO	3.13	3.45	1.63	2.63	2.97	2.83	2.15	2.79	1.81	1.06	1.55
MnO	0.12	0.12	0.03	0.14	0.10	0.09	0.05	0.09	0.05	0.04	0.07

Appendix 3 Pyroxene microprobe data and structural formulae based on 6 oxygen

Appendix 3. Pyroxene microprobe data and structural formulae based on 6 oxygen.											
MgO	16.84	16.68	17.69	17.47	17.23	17.18	17.47	17.30	17.48	18.28	17.51
NiO	0.02	0.03	0.03	0.00	0.03	0.00	0.04	0.01	0.00	0.03	0.00
CaO	24.01	22.88	25.44	25.02	24.17	24.47	25.02	24.72	25.56	26.22	25.59
Na ₂ O	0.25	0.39	0.17	0.03	0.16	0.21	0.12	0.15	0.09	0.05	0.31
K ₂ O	0.00	0.01	0.00	0.00	0.00	0.00	0.00	0.00	0.00	0.00	0.02
Total Oxide %	100.43	100.38	101.22	100.42	100.43	100.81	100.63	101.04	99.63	102.08	101.34
Si	1.94	1.93	1.97	1.98	1.97	1.96	1.98	1.99	1.96	1.99	1.98
Al	0.07	0.13	0.04	0.01	0.05	0.05	0.03	0.02	0.02	0.01	0.03
Ti	0.01	0.01	0.00	0.00	0.00	0.01	0.00	0.00	0.00	0.00	0.00
Cr	0.01	0.01	0.01	0.00	0.01	0.01	0.00	0.00	0.00	0.00	0.00
Fe ³⁺	0.02	0.02	0.02	0.02	0.01	0.02	0.01	0.00	0.05	0.01	0.02
Mg	0.91	0.90	0.94	0.94	0.93	0.92	0.94	0.93	0.95	0.97	0.93
Fe ²⁺	0.07	0.09	0.03	0.06	0.08	0.07	0.05	0.09	0.00	0.02	0.02
Mn	0.00	0.00	0.00	0.00	0.00	0.00	0.00	0.00	0.00	0.00	0.00
Ni	0.00	0.00	0.00	0.00	0.00	0.00	0.00	0.00	0.00	0.00	0.00
Ca	0.93	0.89	0.98	0.97	0.94	0.95	0.97	0.95	1.00	1.00	0.98
Na	0.02	0.03	0.01	0.00	0.01	0.01	0.01	0.01	0.01	0.00	0.02
K	0.00	0.00	0.00	0.00	0.00	0.00	0.00	0.00	0.00	0.00	0.00
Sum	4.00	4.00	4.00	4.00	4.00	4.00	4.00	4.00	4.00	4.00	4.00
Wo %	48.04	46.81	49.54	48.59	47.82	48.31	49.01	48.43	49.79	49.93	49.96
En %	46.88	47.49	47.93	47.21	47.43	47.19	47.62	47.16	47.38	48.43	47.57
Fs %	5.08	5.70	2.53	4.20	4.75	4.50	3.37	4.41	2.84	1.64	2.47

Appendix 4 Garnet microprobe data and structural formulae based on 12 oxygen

Appendix 4. Garnet microprobe data and structural formulae based on 12 oxygen.												
Sample	MC1_4	MC1_12	MC1_13	MC1_15	MC1_20	MC1_21	MC1_22	MC1_23	MC1_24	MC1_25	MC1_31	MC1_32
SiO ₂	37.21	37.05	37.45	37.60	37.82	37.25	37.36	37.74	37.17	37.12	36.85	37.54
TiO ₂	0.58	0.17	0.17	0.24	0.23	0.18	0.16	0.16	0.27	0.33	0.08	0.13
Al ₂ O ₃	16.58	17.98	17.93	18.13	18.05	18.18	18.09	17.86	18.28	18.25	17.30	18.14
Cr ₂ O ₃	0.13	0.02	0.02	0.00	0.01	0.00	0.02	0.03	0.02	0.04	0.00	0.01
MgO	2.91	2.82	2.94	2.60	2.94	2.89	2.71	2.75	2.42	2.56	4.50	2.98
FeO	3.27	2.24	1.92	2.06	1.86	1.78	2.04	2.10	1.81	1.78	3.15	2.06
MnO	0.04	0.08	0.06	0.03	0.10	0.08	0.09	0.08	0.02	0.04	0.06	0.06
CaO	36.51	36.44	36.55	36.85	36.55	36.56	36.78	36.79	36.74	36.71	34.79	36.19
Na ₂ O	0.02	0.01	0.04	0.00	0.00	0.01	0.00	0.00	0.00	0.02	0.00	0.02
K ₂ O	0.01	0.00	0.00	0.00	0.00	0.01	0.00	0.00	0.00	0.00	0.00	0.00
Total Oxide %	97.25	96.80	97.08	97.52	97.56	96.95	97.26	97.51	96.72	96.84	96.73	97.14
Si	5.75	5.72	5.76	5.77	5.79	5.74	5.74	5.79	5.75	5.73	5.67	5.77
Ti	0.07	0.02	0.02	0.03	0.03	0.02	0.02	0.02	0.03	0.04	0.01	0.01
Al	3.02	3.27	3.25	3.28	3.26	3.30	3.28	3.23	3.33	3.32	3.14	3.29
Cr	0.02	0.00	0.00	0.00	0.00	0.00	0.00	0.00	0.00	0.00	0.00	0.00
Fe ³⁺	0.00	0.00	0.00	0.00	0.00	0.00	0.00	0.00	0.00	0.00	0.00	0.00
Mg	0.67	0.65	0.67	0.59	0.67	0.66	0.62	0.63	0.56	0.59	1.03	0.68
Fe	0.42	0.29	0.25	0.26	0.24	0.23	0.26	0.27	0.23	0.23	0.41	0.26
Mn	0.01	0.01	0.01	0.00	0.01	0.01	0.01	0.01	0.00	0.00	0.01	0.01
Ca	6.04	6.03	6.02	6.06	6.00	6.03	6.06	6.05	6.09	6.07	5.74	5.96
Na	0.00	0.00	0.01	0.00	0.00	0.00	0.00	0.00	0.00	0.01	0.00	0.01
K	0.00	0.00	0.00	0.00	0.00	0.00	0.00	0.00	0.00	0.00	0.00	0.00
Total cation	16.00	16.00	16.00	16.00	16.00	16.00	16.00	16.00	16.00	16.00	16.00	16.00
Pyrope %	9.38	9.30	9.70	8.59	9.70	9.57	8.93	9.04	8.11	8.54	14.37	9.87

Appendix 5 Talc microprobe data and structural formulae based on 22 oxygen

Appendix 4. Garnet microprobe data and structural formulae based on 12 oxygen.												
Almandine %	5.92	4.15	3.55	3.82	3.44	3.31	3.77	3.87	3.40	3.33	5.64	3.83
Spessartine %	0.07	0.15	0.11	0.06	0.19	0.15	0.17	0.15	0.03	0.07	0.11	0.12
Grossular %	84.62	86.40	86.64	87.53	86.67	86.97	87.12	86.93	88.46	88.05	79.87	86.18

Appendix 5. Talc microprobe data and structural formulae based on 22 oxygen.		
Sample	MT5_1	MT5_2
SiO ₂	59.15	59.20
TiO ₂	1.21	0.72
Al ₂ O ₃	21.08	20.67
FeO	3.47	3.99
MnO	0.02	0.03
MgO	0.34	0.46
CaO	0.34	0.76
Na ₂ O	14.05	13.63
K ₂ O	0.02	0.15
Total Oxide %	99.69	99.60
Si	7.70	7.73
Ti	0.12	0.07
Al	0.05	0.07
Fe	0.37	0.43
Mn	0.00	0.00
Mg	4.09	4.02
Ca	0.05	0.11

Appendix 6 Amphibole microprobe analyses and structural formulae based on 23 oxygen

Appendix 5. Talc microprobe data and structural formulae based on 22 oxygen.

Na		3.55		3.45
K		0.00		0.03
Sum		15.93		15.90

Appendix 6. Amphibole microprobe data and structural formulae based on 23 oxygen.

Sample	MT2_1	MT2_2	MT2_3	MT2_4	MT2_5	MT2_17	MT2_32	MT2_33	MT2_34	MT2_35	MT2_37
SiO ₂	57.84	58.43	58.65	58.53	59.15	52.35	58.52	58.49	58.29	58.24	58.33
TiO ₂	0.01	0.01	0.02	0.01	0.01	0.03	0.02	0.04	0.04	0.01	0.01
Al ₂ O ₃	0.02	0.04	0.03	0.02	0.03	4.90	0.01	0.02	0.03	0.01	0.02
Cr ₂ O ₃	0.02	0.12	0.09	0.08	0.10	0.42	0.06	0.07	0.12	0.13	0.06
FeO	3.55	3.65	3.54	3.50	3.65	3.40	3.81	3.56	3.76	3.54	3.49
MnO	0.06	0.04	0.05	0.05	0.06	0.06	0.05	0.05	0.06	0.03	0.02
MgO	22.43	22.54	22.49	22.48	22.76	22.05	22.60	22.47	22.31	22.69	22.59
CaO	13.41	13.19	13.33	13.36	13.35	11.35	13.24	13.20	13.34	13.31	13.50
Na ₂ O	0.14	0.17	0.22	0.16	0.18	2.56	0.24	0.24	0.20	0.23	0.16
K ₂ O	0.03	0.05	0.04	0.04	0.04	0.07	0.07	0.05	0.07	0.05	0.05
Total Oxide %	97.52	98.24	98.47	98.23	99.32	97.19	98.62	98.19	98.21	98.24	98.22
Si	7.91	8.01	7.99	8.04	8.03	7.93	9.04	9.03	9.29	8.28	7.97
Al	0.00	0.01	0.00	0.00	0.00	0.88	0.00	0.00	0.01	0.00	0.00
Ti	0.00	0.00	0.00	0.00	0.00	0.00	0.00	0.00	0.00	0.00	0.00
Cr	0.00	0.01	0.01	0.01	0.01	0.05	0.01	0.01	0.02	0.02	0.01
Mg	4.57	4.60	4.57	4.60	4.61	4.98	5.21	5.17	5.30	4.81	4.60
Fe	0.01	0.49	0.33	0.59	0.57	4.25	6.57	6.39	8.02	2.21	0.32
Mn	0.01	0.00	0.01	0.01	0.01	0.01	0.01	0.01	0.01	0.00	0.00
Ca	1.96	1.94	1.95	1.97	1.94	1.84	2.19	2.18	2.28	2.03	1.98

Appendix 7 Chromite microprobe data and structural formulae based on 4 oxygen

Appendix 6. Amphibole microprobe data and structural formulae based on 23 oxygen.										
Na	0.04	0.04	0.06	0.04	0.05	0.75	0.07	0.07	0.06	0.06
K	0.01	0.01	0.01	0.01	0.01	0.01	0.01	0.01	0.01	0.01
Sum	14.91	15.05	15.00	15.08	15.07	16.89	17.03	16.96	17.49	15.64
										15.01
Mg#	1.00	0.90	0.93	0.89	0.89	0.54	0.44	0.45	0.40	0.69
										0.94

Appendix 7. Chromite microprobe data and structural formulae based on 4 oxygen.														
	MS10_2	MS10_4	MS10_8	MS6_1	MS6_12	MS6_35	MS6_36	*SE_1	*SE_2	*SE_5	*SE_6	*SE_9	*SE_13	*SE_15
TiO ₂	0.48	0.20	0.59	0.26	0.17	0.16	0.18	0.20	0.35	0.31	0.29	0.22	0.26	0.27
Al ₂ O ₃	0.16	0.07	0.69	0.10	0.18	0.71	0.69	28.08	26.27	28.32	25.60	23.81	26.32	26.66
Cr ₂ O ₃	30.61	13.35	33.53	26.77	31.76	29.22	31.41	40.21	41.26	38.84	41.83	42.45	41.38	41.98
FeO	59.66	80.29	56.03	56.00	46.43	45.36	49.18	15.58	16.81	16.44	15.50	15.61	17.59	17.20
MnO	1.27	0.45	1.42	6.56	10.11	8.16	5.53	0.39	0.38	0.53	0.19	0.00	0.00	0.00
MgO	0.63	0.34	0.48	2.31	4.20	6.80	5.44	14.36	13.30	13.84	15.88	14.98	13.53	14.14
ZnO	1.04	0.29	1.23	0.42	0.82						0.00	0.18	0.27	0.18
Total Oxide %	93.85	94.99	93.97	92.42	93.68	90.40	92.44	98.82	98.37	98.28	99.44	97.38	99.44	100.54
Ti	0.01	0.01	0.02	0.01	0.00	0.00	0.01	0.00	0.01	0.01	0.01	0.01	0.01	0.01
Al	0.01	0.00	0.03	0.00	0.01	0.03	0.03	0.99	0.95	1.01	0.90	0.86	0.94	0.94
Cr	0.94	0.40	1.03	0.82	0.94	0.88	0.93	0.96	1.00	0.93	0.99	1.03	0.99	0.99
Fe ³⁺	1.03	1.58	0.91	1.16	1.04	1.08	1.02	0.04	0.04	0.05	0.10	0.09	0.06	0.06
Fe ²⁺	0.91	0.96	0.91	0.65	0.42	0.36	0.52	0.35	0.39	0.37	0.29	0.31	0.39	0.37
Mn	0.04	0.01	0.05	0.21	0.32	0.26	0.18	0.01	0.01	0.01	0.00	0.00	0.00	0.00
Mg	0.04	0.02	0.03	0.13	0.24	0.38	0.31	0.64	0.61	0.62	0.71	0.69	0.61	0.63
Zn	0.03	0.01	0.04	0.01	0.02	0.00	0.00	0.00	0.00	0.00	0.00	0.01	0.00	0.00
Total	3.00	3.00	3.00	3.00	3.00	3.00	3.00	3.00	3.00	3.00	3.00	3.00	3.00	3.00

Appendix 8 Magnetite microprobe data and structural formulae based on 4 oxygen

Appendix 7. Chromite microprobe data and structural formulae based on 4 oxygen.

Mg/(Mg+Fe ²⁺)	0.04	0.02	0.03	0.17	0.36	0.52	0.37	0.65	0.61	0.63	0.71	0.69	0.61	0.63
Al/(Al+Fe ³⁺ +Cr)	0.00	0.00	0.02	0.00	0.00	0.02	0.02	0.50	0.48	0.51	0.45	0.43	0.47	0.47
Cr/(Cr+Al)	0.99	0.99	0.97	0.99	0.99	0.97	0.97	0.49	0.51	0.48	0.52	0.54	0.51	0.51
*Data from [10]														

Appendix 8. Magnetite microprobe data and structural formulae based on 4 oxygen.

Sample	MS10_1	MS10_9	MS10_10	MS6_2	MS6_3	MS6_4	MS6_6	MS6_7	MS6_8	MS6_9	MS6_10	MS6_11	CNS2_1	MS6_1b	MS6_15	MS6_16	MS6_17	MS6_18	MS6_19	MS6_20	MS6_21	MS6_22
TiO ₂	0.19	0.20	0.12	0.04	0.20	0.09	0.10	0.00	0.11	0.19	0.17	0.12	0.05	0.04	0.02	0.00	0.01	0.04	0.03	0.02	0.08	
Al ₂ O ₃	0.02	0.14	0.00	0.01	0.00	0.02	0.04	0.00	0.01	0.00	0.04	0.00	0.03	0.00	0.00	0.00	0.00	0.16	0.05	0.03	0.01	
Cr ₂ O ₃	13.23	13.22	11.09	5.40	19.61	9.73	12.63	4.63	13.76	21.78	19.51	15.95	7.07	5.53	11.47	0.74	2.47	9.99	4.16	7.61	9.57	
FeO	80.84	80.15	81.42	86.75	68.85	80.71	76.98	86.49	76.34	65.91	69.72	74.62	87.10	84.62	78.71	89.02	87.45	68.46	84.00	78.51	80.16	
MnO	0.45	0.42	0.33	0.40	3.11	1.20	2.10	0.55	2.05	3.71	3.00	2.47	0.51	1.20	2.43	0.33	0.74	2.96	0.70	1.94	1.16	
MgO	0.21	0.40	0.93	0.73	1.44	1.14	1.15	0.90	1.28	1.44	1.49	1.30	0.73	1.68	1.56	1.21	1.18	3.62	1.64	1.83	1.04	
ZnO	0.28	0.27	0.25	0.00	0.26	0.12	0.20	0.00	0.14	0.28	0.23	0.16	0.07	0.12	0.11	0.00	0.05	0.39	0.02	0.15	0.03	
Total Oxide %	95.23	94.79	94.15	93.33	93.48	93.00	93.20	92.58	93.69	93.31	94.16	94.61	95.56	93.18	94.30	91.30	91.90	85.62	90.59	90.09	92.04	
Ti	0.01	0.01	0.00	0.00	0.01	0.00	0.00	0.00	0.01	0.00	0.00	0.00	0.00	0.00	0.00	0.00	0.00	0.00	0.00	0.00	0.00	
Al	0.00	0.01	0.00	0.00	0.00	0.00	0.00	0.00	0.00	0.00	0.00	0.00	0.00	0.00	0.00	0.00	0.01	0.00	0.00	0.00	0.00	
Cr	0.40	0.40	0.33	0.16	0.59	0.30	0.38	0.14	0.42	0.66	0.59	0.48	0.21	0.17	0.34	0.02	0.08	0.32	0.13	0.24	0.29	
Fe ³⁺	1.59	1.59	1.66	1.83	1.39	1.70	1.61	1.86	1.58	1.33	1.40	1.52	1.79	1.83	1.66	1.98	1.92	1.67	1.87	1.76	1.70	
Fe ²⁺	0.97	0.96	0.93	0.95	0.82	0.89	0.86	0.93	0.86	0.79	0.82	0.85	0.94	0.86	0.83	0.92	0.91	0.67	0.88	0.82	0.90	
Mn	0.01	0.01	0.01	0.01	0.10	0.04	0.07	0.02	0.07	0.12	0.10	0.08	0.02	0.04	0.08	0.01	0.02	0.10	0.02	0.06	0.04	
Mg	0.01	0.02	0.05	0.04	0.08	0.07	0.07	0.05	0.07	0.08	0.08	0.07	0.04	0.10	0.09	0.07	0.07	0.22	0.10	0.11	0.06	
Zn	0.01	0.01	0.01	0.00	0.01	0.00	0.01	0.00	0.00	0.01	0.01	0.00	0.00	0.00	0.00	0.00	0.01	0.00	0.00	0.00	0.00	
Total	3.00	3.00	3.00	3.00	3.00	3.00	3.00	3.00	3.00	3.00	3.00	3.00	3.00	3.00	3.00	3.00	3.00	3.00	3.00	3.00	3.00	

Appendix 9 Pentlandite microprobe data

Appendix 8. Magnetite microprobe data and structural formulae based on 4 oxygen.

Mg/(Mg+Fe ²⁺)	0.01	0.02	0.05	0.04	0.09	0.07	0.07	0.05	0.08	0.09	0.09	0.08	0.04	0.10	0.10	0.07	0.07	0.25	0.10	0.12	0.06
Al/(Al+Fe ³⁺ +Cr)	0.00	0.00	0.00	0.00	0.00	0.00	0.00	0.00	0.00	0.00	0.00	0.00	0.00	0.00	0.00	0.00	0.00	0.00	0.00	0.00	0.00
Cr/(Cr+Al)	1.00	0.98	1.00	1.00	1.00	1.00	1.00	1.00	1.00	1.00	1.00	1.00	0.99	1.00	1.00	1.00	1.00	0.98	0.99	0.99	1.00

Appendix 9. Pentlandite microprobe data.

Comment	MS10_14	MS10_16	MS10_17	MS6_32	MS6_33	MS6_34
SiO ₂	3.38	3.36	1.81	0.05	0.00	0.17
TiO ₂	0.00	0.00	0.01	0.00	0.00	0.00
Al ₂ O ₃	0.06	0.10	0.05	0.00	0.00	0.00
FeO	36.73	37.13	39.66	31.77	32.06	32.21
Cr ₂ O ₃	0.03	0.04	0.01	0.00	0.00	0.01
MnO	0.00	0.02	0.00	0.00	0.01	0.00
MgO	4.65	4.80	2.40	0.03	0.01	0.08
Na ₂ O	0.01	0.04	0.06	0.00	0.01	0.00
CaO	0.00	0.00	0.00	0.00	0.00	0.00
K ₂ O	0.01	0.00	0.00	0.00	0.00	0.00
Total Oxide %	44.87	45.48	44.00	31.86	32.08	32.47

Appendix 10. Whole rock geochemical data.

Sample	MS1	MS2	MS3	MS4	MS5	MS7	MS8	MS9	MS10	MS11	MC1	MT1	MT2	MT3	MT4
SiO ₂	41.46	43.44	45.06	40.92	40.16	36.17	39.43	5.87	38.18	42.76	40.32	42.85	29.41	61.35	30.79
TiO ₂	0.03	0.03	0.01	0.13	0.02	0.03	0.02	0.01	0.02	0.02	0.11	0.01	0.03	0.01	0.94
Al ₂ O ₃	1.23	1.38	0.76	13.42	1.14	1.01	1.14	0.05	1.51	0.97	13.80	1.17	0.84	0.08	18.81

Appendix 10 Whole rock geochemical data

Appendix 10. Whole rock geochemical data.															
Fe ₂ O ₃	7.58	3.85	3.05	2.93	5.83	12.47	5.28	0.87	7.46	8.31	2.66	7.20	5.44	4.12	10.89
MnO	0.03	0.23	0.10	0.12	0.08	0.05	0.05	0.55	0.11	0.05	0.13	0.09	0.18	0.03	0.21
MgO	35.39	36.48	37.55	15.70	37.38	35.78	39.11	23.95	34.83	33.87	15.41	33.31	19.52	25.84	26.02
CaO	0.01	0.01	0.01	21.57	0.10	0.07	0.20	25.67	2.34	0.01	22.19	0.96	20.50	2.03	0.25
Na ₂ O	0.01	0.01	0.01	0.05	0.01	0.01	0.01	0.01	0.01	0.01	0.04	0.01	0.07	0.01	0.01
K ₂ O	0.01	0.01	0.01	0.01	0.01	0.02	0.04	0.01	0.01	0.01	0.01	0.01	0.01	0.01	0.01
P ₂ O ₅	0.01	0.01	0.01	0.01	0.01	0.02	0.01	0.01	0.01	0.01	0.01	0.01	0.01	0.01	0.19
Cr ₂ O ₃	0.42	0.81	0.02	0.10	0.30	0.47	0.13	0.01	0.35	0.44	0.09	0.28	0.34	0.00	0.01
LOI	13.00	12.70	12.90	4.80	14.20	12.90	13.70	42.60	14.40	12.70	5.00	3.37	0.02	0.34	0.03
Mg#	90.25	94.94	96.06	91.39	92.70	85.04	93.62	98.20	90.25	88.98	68.88	90.17	87.67	92.55	82.56
Sum	99.41	99.34	99.39	99.73	99.39	99.39	99.33	99.57	99.39	99.39	99.74	99.44	99.64	99.59	99.43
Trace elements															
Cr	2846.7 0	5542.8 6	130.0 2	684.3 0	2073.4 4	3195.7 0	903.2 8	2408.7 95.80	3017.7 5	588.4 8	1895.5 1	2319.7 2	13.69 9	82.12	
Ni	0.42	0.81	0.02	0.10	0.30	0.47	0.13	0.01	1988.0	2610.0	210.0	2094.0	1337.0	234.0	159.0
Co	1.00	1.00	1.00	1.00	1.00	3.00	3.00	2.00	91.40	100.10	17.60	93.40	61.30	18.80	26.60
V	0.10	0.10	0.10	0.10	0.10	0.10	0.10	1.00	48.00	44.00	89.00	25.00	35.00	11.00	210.0
Cu	0.10	0.30	0.10	0.10	0.10	0.20	0.20	0.30	13.90	23.90	36.70	5.40	24.10	9.70	2.70
Pb	4.70	12.30	45.30	26.10	0.10	1.90	1.50	0.20	0.50	0.80	1.00	13.80	0.70	0.10	1.30
Zn	1.10	3.80	0.10	0.40	0.10	1.20	1.20	0.20	29.00	35.00	8.00	24.00	14.00	1.00	101.0
Rb	0.10	0.10	0.10	0.20	0.10	1.60	1.80	0.40	1.00	0.40	0.20	0.10	0.20	0.10	0.30
Ba	99.41	99.34	99.39	99.73	99.39	99.39	99.33	99.57	9.00	5.00	5.00	1.00	3.00	1.00	5.00
Sr	1.00	1.00	1.00	1.00	1.00	1.00	1.00	1.00	23.00	1.50	7.40	24.90	184.00	4.00	8.70
Ga	0.10	0.10	0.10	0.10	0.10	0.10	0.10	0.10	1.70	2.20	4.70	2.10	1.30	0.50	16.60
Nb	0.10	0.10	0.10	0.10	0.10	1.10	0.70	0.10	1.80	2.50	0.10	0.40	0.10	0.10	14.80

Appendix 10. Whole rock geochemical data.															
Hf	1.00	1.80	0.60	4.50	0.90	1.30	1.20	0.80	0.10	0.10	0.10	0.10	0.10	0.10	5.80
Cs	98.90	280.50	24.20	20.70	80.50	140.00	62.30	4.90	0.40	0.10	0.10	0.10	0.10	0.10	0.10
Ta	0.60	0.50	0.50	7.50	0.50	1.90	13.50	231.6 0	0.10	0.10	0.10	0.10	0.10	0.10	1.00
Th	0.10	0.10	0.10	0.10	0.10	1.60	0.50	0.40	0.20	0.20	0.20	0.20	0.20	0.20	20.90
U	0.20	0.20	0.20	0.20	0.20	0.20	0.20	0.20	0.10	0.10	0.10	0.10	0.10	0.10	2.80
Zr	3.00	0.80	0.50	0.50	3.60	6.70	1.30	0.90	0.10	0.10	2.60	0.20	1.70	0.30	216.8
Y	0.30	2.40	0.10	3.30	0.10	59.60	13.20	2.60	0.50	2.50	2.80	1.50	4.60	0.80	31.40
Rare Earth Elements															
La	0.80	0.90	0.20	3.80	0.80	1.10	0.30	1.10	0.20	0.40	0.70	0.20	0.80	0.10	95.10
Ce	0.10	0.30	0.10	0.80	0.20	0.90	0.80	1.30	0.30	1.10	1.30	0.40	1.60	0.30	181.2
Pr	0.30	0.80	0.10	1.90	0.20	1.00	1.00	1.60	0.08	0.20	0.20	0.08	0.27	0.07	19.40
Nd	0.06	0.10	0.02	0.30	0.02	0.12	0.04	0.22	0.30	0.80	1.20	0.60	1.90	0.30	67.50
Sm	0.30	0.30	0.30	1.20	0.30	1.00	0.70	1.10	0.05	0.14	0.32	0.17	0.41	0.11	11.30
Eu	0.09	0.15	0.05	0.43	0.05	0.06	0.13	0.35	0.02	0.08	0.53	0.04	0.13	0.02	1.95
Gd	0.04	0.03	0.03	0.58	0.03	0.02	0.02	0.10	0.05	0.21	0.39	0.19	0.60	0.13	8.70
Tb	0.08	0.24	0.10	0.56	0.10	0.09	0.05	0.30	0.01	0.01	0.08	0.04	0.11	0.03	1.06
Dy	0.02	0.03	0.01	0.10	0.01	0.02	0.01	0.04	0.05	0.25	0.48	0.18	0.68	0.23	6.00
Ho	0.15	0.30	0.05	0.66	0.09	0.16	0.05	0.27	0.03	0.06	0.10	0.05	0.15	0.05	0.95
Er	0.03	0.03	0.02	0.10	0.03	0.07	0.02	0.03	0.03	0.18	0.30	0.16	0.38	0.12	2.79
Tm	0.07	0.11	0.07	0.34	0.10	0.07	0.06	0.03	0.01	0.01	0.05	0.03	0.06	0.02	0.48
Yb	0.01	0.03	0.01	0.06	0.01	0.03	0.01	0.02	0.05	0.25	0.29	0.20	0.39	0.12	3.42
Lu	0.14	0.23	0.05	0.35	0.08	0.07	0.05	0.05	0.01	0.02	0.04	0.03	0.06	0.03	0.51